iScience

CellPress

Article

CNTF and Nrf2 Are Coordinately Involved in Regulating Self-Renewal and Differentiation of Neural Stem Cell during Embryonic Development

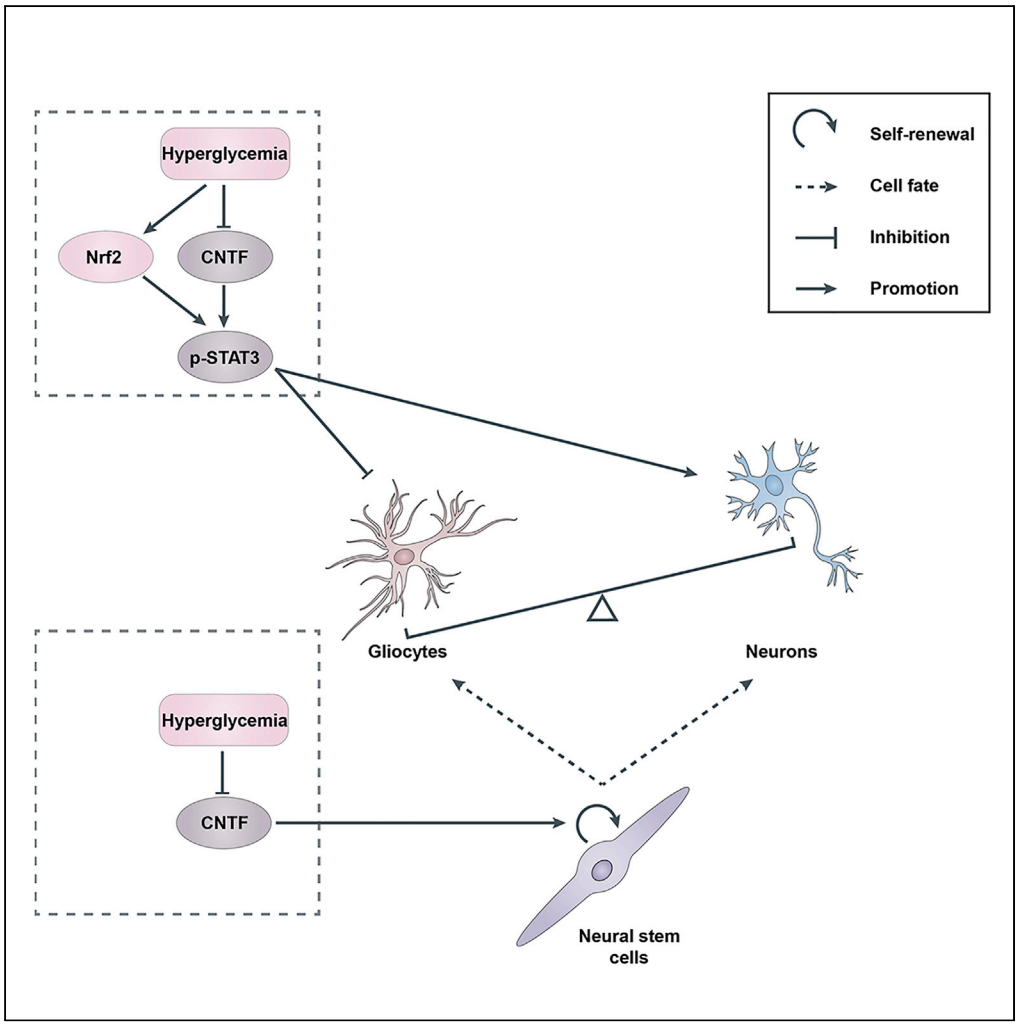

Zhen-Peng Si, Guang Wang, Sha-Sha Han, ..., Beate Brand-Saberi, Xuesong Yang, Guo-Sheng Liu

yang_xuesong@126.com (X.Y.)
tlgs@jnu.edu.cn (G.-S.L.)

HIGHLIGHTS

Hyperglycemia affects self-renewal ability of neural progenitor cells

Hyperglycemia twists the developmental switch from neurogenesis into gliogenesis

CNTF regulates hyperglycemia-induced imbalance between neurogenesis and gliogenesis

CNTF and Nrf2 co-ordinately regulate neural development through p-STAT3

Si et al., iScience 19, 303–315
September 27, 2019
https://doi.org/10.1016/j.isci.2019.07.038

iScience

CellPress

Article

CNTF and Nrf2 Are Coordinately Involved in Regulating Self-Renewal and Differentiation of Neural Stem Cell during Embryonic Development

Zhen-Peng Si,[1,5] Guang Wang,[2,5] Sha-Sha Han,[1] Ya Jin,[1] Yu-Xuan Hu,[2] Mei-Yao He,[1] Beate Brand-Saberi,[3] Xuesong Yang,[2,4,6,*] and Guo-Sheng Liu[1,*]

SUMMARY

There is high risk of fetal neurodevelopmental defects in pregestational diabetes mellitus (PGDM). However, the effective mechanism of hyperglycemia-induced neurodevelopmental negative effects, including neural stem cell self-renewal and differentiation, still remains obscure. Neuropoietic cytokines have been shown to play a vital part during nervous system development and in the coordination of neurons and gliocytes. Nuclear factor (erythroid-derived 2)-like 2 (Nrf2) dysfunction might be related to a reduction of self-protective response in brain malformation induced by hyperglycemia. We therefore evaluated the role of Nrf2 and neuropoietic cytokines in fetal neurodevelopmental defects induced by PGDM and determined the mechanisms involved. Our data reveal that PGDM dramatically impairs the developmental switch of neural stem cells from neurogenesis to gliogenesis, principally under the cooperative mediation of neuropoietic cytokine CNTF and Nrf2 antioxidative signaling. This indicates that CNTF and Nrf2 could be potentially used in the prevention or therapy of neurodevelopmental defects of PGDM offspring.

INTRODUCTION

The risk of birth defects in the newborns of pregnant women with type 1 or type 2 pregestational diabetes mellitus (PGDM) was appreciably higher than the ones of the mother who never suffered from diabetes or gestational diabetes mellitus (Correa et al., 2008). Actually, the frequency of anomalies in the nervous system is 2.7 times higher than the average of congenital malformations induced by hyperglycemia (Corrigan et al., 2009; Macintosh et al., 2006). One of the reasons for the high incidence of congenital anomalies of the nervous system is that neurulation occurs at a very early developmental stage, during which embryos are vulnerable to external harmful factors (Rice and Barone, 2000; Rodier, 1994). The precise mechanism underlying the teratogenesis of the nervous system associated with diabetes is unclear partially because of the complexity. However, maternal hyperglycemia is regarded as a very important teratogen leading to congenital anomalies by generating excess reactive oxygen species (ROS) at the neurula stage (Corrigan et al., 2009; Zangen et al., 2002). In our previous study, we found that neuronal differentiation was suppressed and glial cell lineage differentiation was slightly promoted while it was usually accompanied by an excessive oxidation stress in the embryo brain of PGDM mice, which might lead to maternal hyperglycemia-induced neurodevelopmental defects (Jin et al., 2016).

As an initial phase of nervous system development, neurulation refers to the morphogenetic process by which the neural tube forms in vertebrates. The development of the nervous system is precisely controlled by a complex series of spatiotemporally coordinated signaling pathways (Canning et al., 2008; De Robertis and Kuroda, 2004; Timmer et al., 2002; Wilson and Maden, 2005; Zirra et al., 2016). The cell fate toward two subpopulations of neuronal and astroglial cells will depend on the cell localization, in which cells respond to a spatial morphogen concentration (Du and Zhang, 2004). The subpopulation of neuronal or glial lineage can be identified using their respective markers, for example, neurons can be determined by neurofilament protein, whereas astrocytes can be identified by glial fibrillary acidic protein (GFAP) (Regan, 1988). As a potent neural factor, ciliary neurotrophic factor (CNTF) was originally identified as a crucial factor to maintain chicken neuron survival *in vitro* (Adler et al., 1979; Varon et al., 1979). CNTF acts as one of the key neuropoietic cytokines, which concertedly modulate neuronal and glial cell differentiation and responses to exogenous stimuli (Bauer et al., 2007). Janus-activated kinase-signal

[1]Department of Pediatrics, The First Affiliated Hospital, Jinan University, Guangzhou 510630, China

[2]International Joint Laboratory for Embryonic Development & Prenatal Medicine, Division of Histology and Embryology, Medical College, Jinan University, Guangzhou 510632, China

[3]Department of Anatomy and Molecular Embryology, Ruhr University Bochum, Bochum, Germany

[4]Key Laboratory for Regenerative Medicine of the Ministry of Education, Jinan University, Guangzhou 510632, China

[5]These authors contributed equally

[6]Lead Contact

*Correspondence: yang_xuesong@126.com (X.Y.), tlgs@jnu.edu.cn (G.-S.L.)

https://doi.org/10.1016/j.isci.2019.07.038

transducer, activator of transcription (JAK-STAT) is the major signaling transduction pathway for these neuropoietic cytokines including CNTF to exert their function (Bauer et al., 2007).

ROS plays a crucial role in regulating the redox reactions in a variety of signaling pathways (Giordano, 2005; Murdoch et al., 2006; Sawyer et al., 2002). Excessive ROS generation is often associated with pathologic disorders because ROS act as primary and secondary messengers to promote cell death (Giordano, 2005; Murdoch et al., 2006; Sawyer et al., 2002), through damaging macromolecules such as proteins, lipids, and DNA (Valko et al., 2007). Accumulating evidence suggests that excess ROS exert a teratogenic effect on developing embryos and fetuses, such as neurodevelopmental defects (Wells et al., 2009). Obviously, a delicate balance between ROS production and detoxification is indispensible for maintaining normal cellular functions (Karbownik and Lewinski, 2003; Singal et al., 2001). Nrf2 is a Cap'n'Collar basic leucine zipper transcription factor that protects cells from oxidative or electrophilic stress by regulating cellular redox homeostasis (Giordano, 2005; Zhang, 2006). In the presence of oxidative stress, Nrf2 eventually activates transcription by specifically binding to the antioxidant response element of its target gene promoters (Rushmore and Pickett, 1990). Heme oxygenase 1 (HO1) and NAD(P)H quinone oxidoreductase 1 (NQO1) have been identified as vital genes involved in regulating Nrf2 expression (Jaiswal, 2004). Keap1 is a principal repressor of Nrf2 via ubiquitination (Itoh et al., 2010).

Therefore, in this study, we mainly committed to exploring how hyperglycemia affects the self-renewal and differentiation of neural stem cells during embryo development, using the streptozotocin (STZ)-induced PGDM mouse model and numerous corresponding cell lines.

RESULTS

The Probability of Neurodevelopmental Defects Is Augmented in PGDM Mouse Fetuses

A mouse model of PGDM was established by intraperitoneal injection of STZ (Figure S1A), and the harvest timings were based on the consideration of key points during neurogenesis and gliogenesis. Blood glucose levels were monitored (Han et al., 2015) to verify that a mouse model of PGDM had been successfully created (Figure S1B). PGDM fetal mice had lower body weights than the ones in control mice at embryonic day (E)12.5, E15.5, and E18.5 (Figure S1C). The phenotypes of morphological abnormality in early developmental PGDM mouse fetuses were principally focused on nervous systems including encephalocele, spina bifida, anencephaly, and fetal resorption (Figures S1D–S1H). Compared with the control, there totally were higher incidences of PGDM fetal abnormality (Figure S1I), in which brain and spinal malformations occurred more frequently than others except for fetal resorption (Figure S1J), suggesting that the diabetic mouse model was successfully established.

PGDM Influences the Molecular Switch of Neural Stem Cells toward Neurogenesis or Gliogenesis at Neural Tube Trunk during Mouse Embryonic Neural Development

The results showed that positive areas of the neuronal marker Tuj1 (β3-tubulin) and NF-M (neurofilament-medium chain) in both E15.5 and E18.5 PGDM fetal trunk neural tubes were significantly less than the ones in control mice, whereas the positive areas of glial cell marker GFAP were dramatically bigger than the ones in control mice, and the positive Olig2 (oligodendrocyte transcription factor 2) cell numbers were much more than the ones in E15.5 and E18.5 control mice, respectively (Figures 1A–1L and S2A–S2J). Meanwhile, western blot and quantitative PCR data also indicated that NF-M and Tuj1 expression at both mRNA and protein levels decreased and GFAP expression was upregulated in both E15.5 and E18.5 PGDM mice compared with controls (Figures 1M–1P and 1M′–1N′), suggesting that the hyperglycemia in PGDM promoted the differentiation of neural stem cells toward glial cells and simultaneously inhibited the differentiation of neural stem cells into neurons (Figure 1Q). The results of E12.5 control and PGDM mouse embryos demonstrated that both NF-M- and Tuj1-labeled neuronal differentiation was also suppressed and the expression of GFAP was increased (Figures S3A–S3L), suggesting that hyperglycemia-induced imbalance of neural differentiation occurs at an early stage of development. The observation was further verified by the results of *in vitro* primary culture of neural stem cells and differentiated cells (see the details in Transparent Methods) as shown in Figures S4A–S4M.

Immunofluorescent staining showed that expression of CNTF was suppressed in E15.5 PGDM mouse neural tube at trunk level compared with control (Figures 2A–2E); moreover, the expression of CT-1 (cardiotrophin-1) (Figures 2F–2J) and LIF (leukemia inhibitory factor) (Figures 2K–2O) was upregulated in E15.5 PGDM mouse neural tubes at trunk level compared with controls (Figures 2F–2O). Meanwhile,

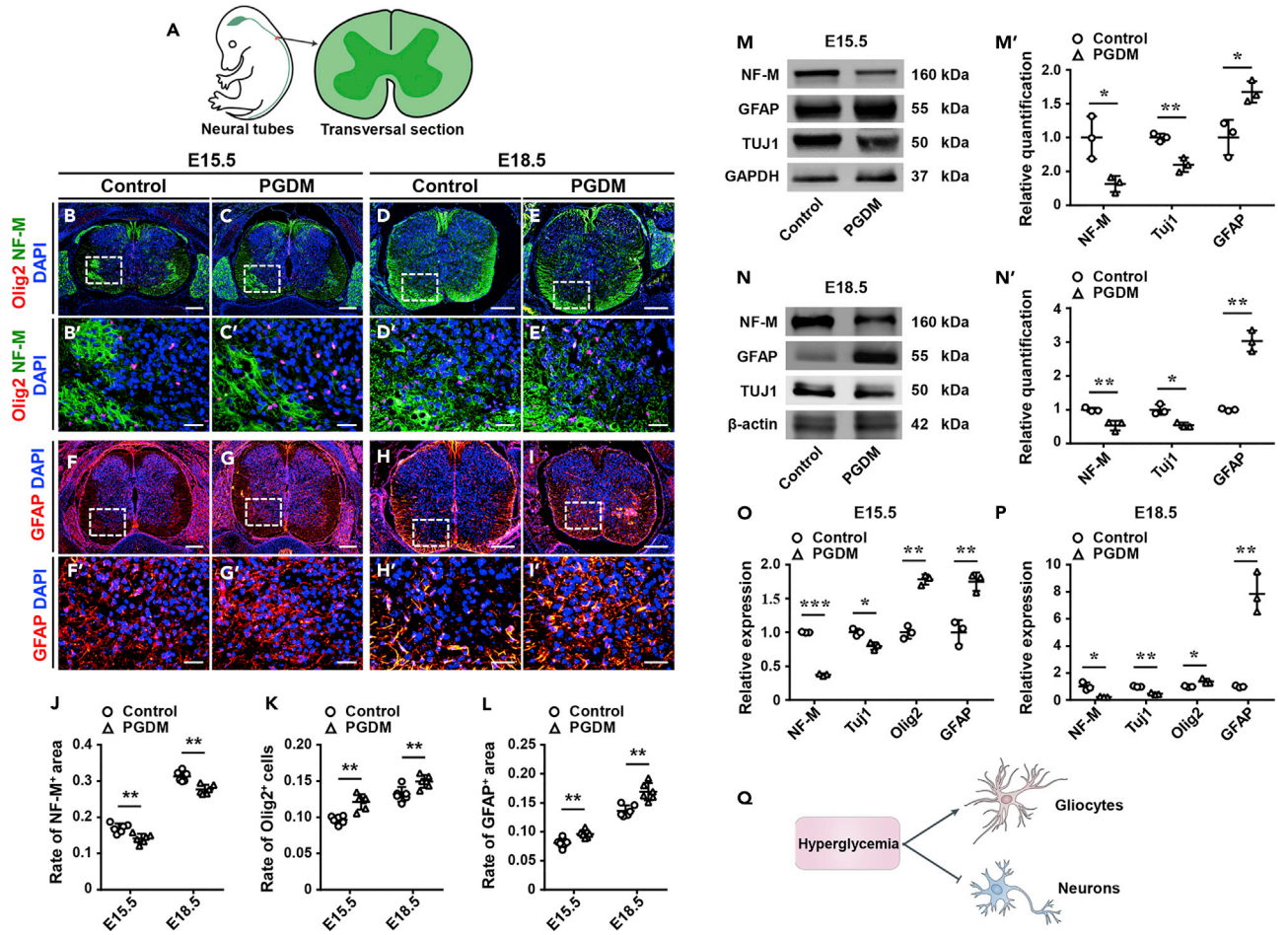

Figure 1. Determination of Crucial Gene Expression of Neuronal Differentiation in the Fetal Trunk Neural Tubes of PGDM Mice

(A) A sketch illustrating the transverse section level of E12.5, E15.5, or E18.5 fetal trunk neural tubes.

(B–I) Olig2 (red) and NF-M (green) double-immunofluorescent staining (B–E) or GFAP immunofluorescent staining (F–I) was performed on the transverse sections of E15.5 (B, C, F, and G) or E18.5 (D, E, H, and I) neural tubes from control (B, D, F, and H) and PGDM (C, E, G, and I) groups. All sections were counterstained with DAPI.

(B′–I′) High-magnification images from the sites indicated by white squares in (B–I), respectively.

(J–L) Bar charts showing the rate comparisons of NF-M$^+$ areas (J), Olig2$^+$ cells (K), and GFAP$^+$ areas (L) between control and PGDM groups.

(M, N, M′, and N′) Western blot data showing the expression of NF-M, Tuj1, and GFAP in E15.5 (M) or E18.5 (N) control and PGDM mouse embryos at protein level, which were quantitatively analyzed in M′–N′.

(O and P) Quantitative PCR data showing the expression of *NF-M*, *Tuj1*, *Olig2*, and *GFAP* in E15.5 (O) or E18.5 (P) control and PGDM mouse embryos at mRNA level.

(Q) A model illustrating the imbalance of neural differentiation induced by hyperglycemia.

For (J, K, and L), n = 6, for (M′, N′, O, and P), n = 3, t test, *p < 0.05, **p < 0.01, ***p < 0.001. Data are represented as mean ± SEM. Scale bars, 500 μm in (B–I) and 100 μm in (B′–I′). See also Figures S1–S4.

quantitative PCR (Figure 2P) and western blot (Figures 2Q and 2R) data displayed that *CNTF* expression was reduced, and CT-1, *LIF*, *interleukin-6* expression was increased in PGDM mice compared with controls at both mRNA and protein levels. These data suggest that CNTF plays an important role in hyperglycemia-induced imbalance of neurogenesis and gliogenesis during neural development (Figure 2S).

PGDM Affects Neural Stem Cell Self-Renewal at Neural Tube Trunk during Mouse Embryonic Neural Development

Next we focused on the potential effect of PGDM on neural stem cell self-renewal because CNTF has been known to be a key factor in all the developmental processes of nervous system (Shimazaki et al., 2001). The

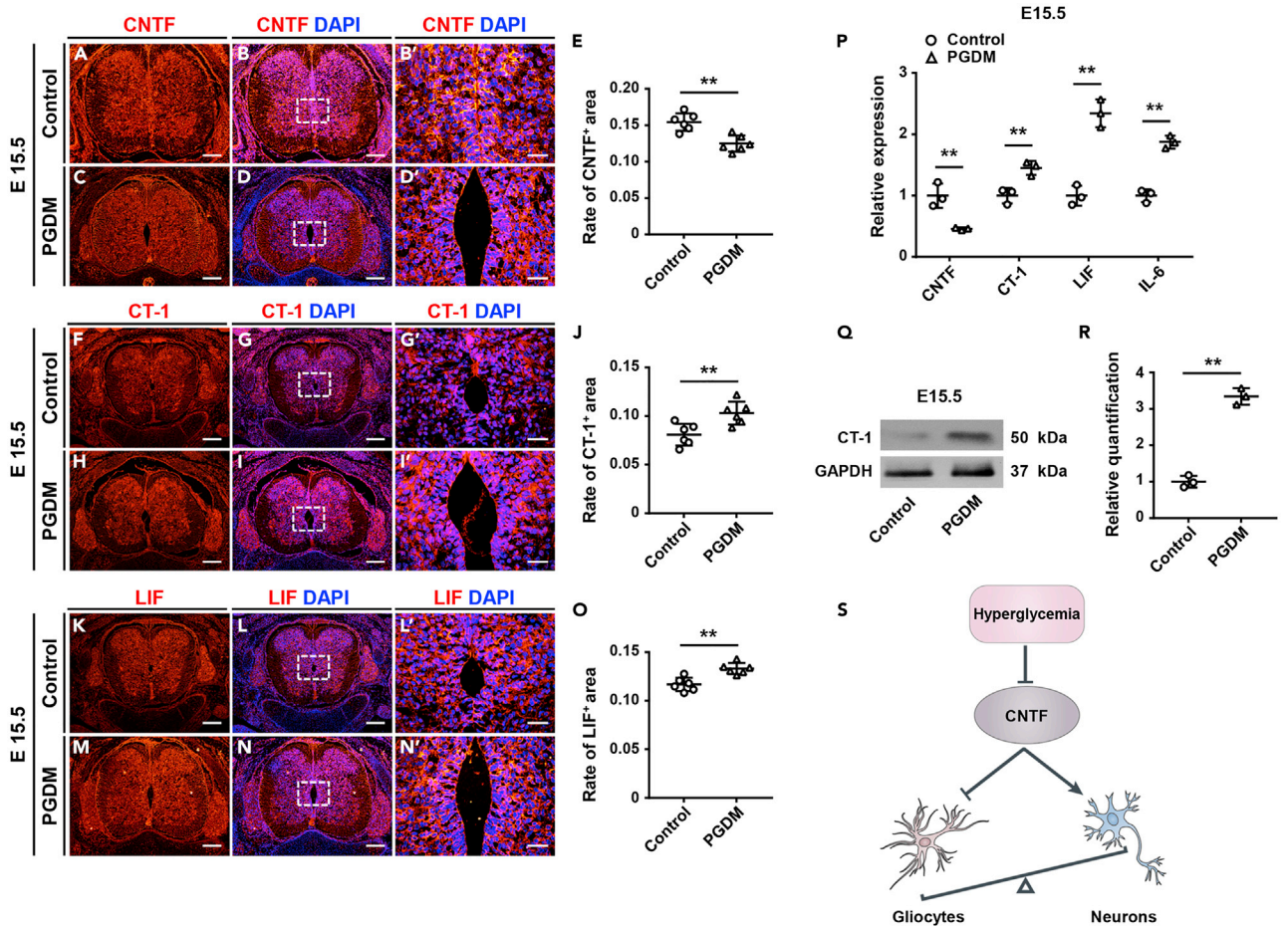

Figure 2. Determining Hyperglycemia-Induced Expression of CNTF, CT-1, and LIF in the Fetal Trunk Neural Tubes of PGDM Mice

(A–D, F–I, and K–N) CNTF (A–D), CT-1 (F–I), or LIF (K–N) immunofluorescent staining was performed on the transverse sections of E15.5 trunk neural tubes from control (A, B, F, G, K, and L) and PGDM (C, D, H, I, M, and N) groups, in which (B, D, G, I, L, and N) were counterstained with DAPI.

(B′, D′, G′, I′, L′, and N′) The high-magnification images from the sites indicated by white squares in (B, D, G, I, L, and N), respectively.

(E, J, and O) Bar charts showing the rate comparisons of CNTF$^+$ areas (E), CT-1$^+$ areas (J), and LIF$^+$ areas (O) between control and PGDM groups.

(P) Quantitative PCR data showing the expression of *CNTF*, *CT-1*, *LIF*, and *interleukin* (*IL*)*-6* in E15.5 control and PGDM mouse embryos at mRNA level.

(Q and R) Western blot data showing the expression of CT-1 in E15.5 control and PGDM mouse embryos at protein level (Q), which was quantitatively analyzed (R).

(S) A sketch describing the mechanism of how hyperglycemia affects neural differentiation.

For (E, J, and O), n = 6, for (P and R), n = 3, t test, **p < 0.01. Data are represented as mean ± SEM. Scale bars, 500 μm in (A–D, F–I, and K–N) and 100 μm in (B′, D′, G′, I′, L′, and N′).

double-immunofluorescent staining of Sox2 (the marker for multipotent neural stem cells and essential transcription factor for maintaining self-renewal) and proliferating cell nuclear antigen (PCNA) was performed on transverse sections of neural tubes of E15.5 and E18.5 control and PGDM mouse embryos at trunk level (Figures 3A–3L), and results demonstrated that both the ratio of Sox2-positive cells in total cells (Figures 3M and 3N) and the ratio of Sox2/PCNA-co-positive cells (Figures 3O and 3P) in Sox2-positive cells significantly decreased in E15.5 and E18.5 PGDM mouse embryonic neural tubes compared with controls. Quantitative PCR data also verified the lower expression of *Sox2* at the mRNA level in both E15.5 and E18.5 PGDM mouse embryonic neural tubes compared with control (Figures 3Q and 3R). The primary culture of neural stem cells *in vitro* (Figures 3S–3U) showed that high glucose (25 mmol/L) could inhibit neurosphere frequency of occurrence and addition of CNTF in culture medium rescued the hyperglycemia-induced reduction (Figure 3V). A similar result was observed in measuring neurosphere sizes (Figure 3W). This suggests that diabetes mellitus does not only influence the neural precursor cell fates toward glial cells but also affects the neural stem cell self-renewal.

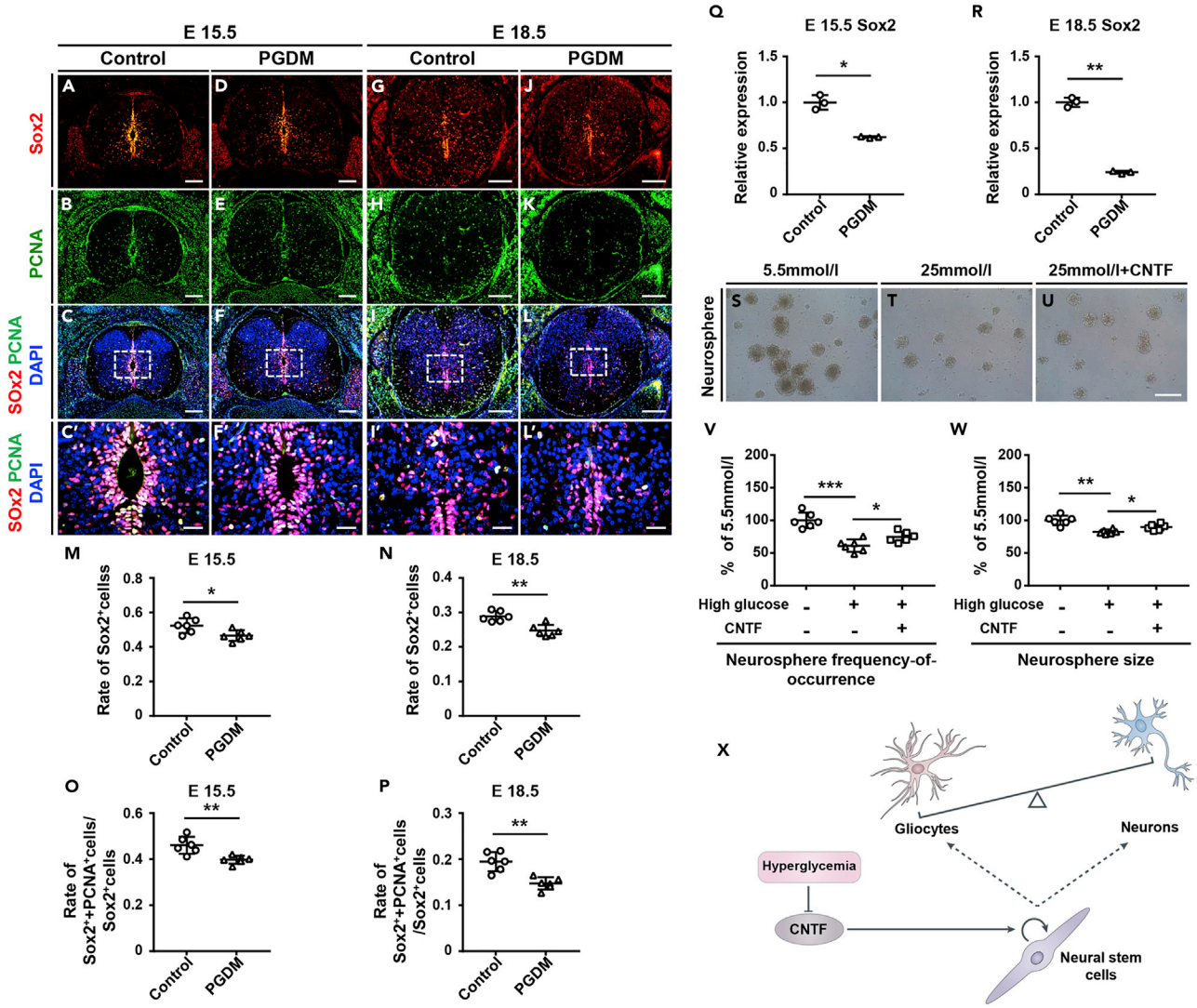

Figure 3. Assessing Hyperglycemia-Induced Self-Renewal of Neural Stem Cells Using *In Vivo* and *In Vitro* Models

(A–L) Sox2 (red, A, D, G, and J) and PCNA (green, B, E, H, and K) double-immunofluorescent staining was performed on the transverse sections of E15.5 (A–F) or E18.5 (G–L) trunk neural tubes from control (A–C and G–I) and PGDM (D–F and J–L) groups, in which (C, F, I, and L) were merged ones from Sox2 and PCNA staining, and then counterstained with DAPI.

(C′, F′, I′, and L′) The high-magnification images from the sites indicated by white squares in (C, F, I, and L), respectively.

(M–P) Bar charts showing the rate comparisons of Sox2-positive cells in total cells (M and N) or Sox2 and PCNA double-positive cells in total Sox2-positive cells (O and P) on the transverse sections between E15.5 (M and O) or E18.5 (N and P) control embryos and PGDM embryos.

(Q and R) Quantitative PCR data showing the expression of *Sox2* in E15.5 (Q) or E18.5 (R) control and PGDM mouse embryos at mRNA level.

(S–U) Representative bright-field images of *in vitro* cultured neurospheres exposed to 5.5 mmol/L D-glucose (S), 25 mmol/L D-glucose (T), or 25 mmol/L D-glucose with CNTF (U).

(V and W) Bar charts showing the percentages of neurosphere frequency-of-occurrence (V) or neurosphere sizes (W) in 25 mmol/L D-glucose and 25 mmol/L D-glucose with CNTF of the neurosphere numbers or sizes in 5.5 mmol/L, which is regarded as 100%.

(X) A model illustrating the influence of hyperglycemia on neural stem cell self-renewal.

For (M–P) and (V–W), n = 6, for (Q and R), n = 3, ANOVA, least significance difference, Student-Newman-Keuls, and t test, *$p < 0.05$, **$p < 0.01$, ***$p < 0.001$. Data are represented as mean ± SEM. Scale bars, 500 μm in (A–L) and (S–U) and 100 μm in (C′, F′, I′, and L′).

PGDM-Induced Neuronal Proliferation Inhibition and Glial Cell Proliferation Enhancement Contribute to the Imbalance between Neurogenesis and Gliogenesis

Double-immunofluorescent staining of NF-M (neuronal marker) and Ki67 (cell proliferation marker) was performed on transverse sections of neural tubes of E15.5 and E18.5 control and PGDM mouse embryos at trunk level (Figures 4A–4D, 4A1–4D1, and 4A2–4D2). Our results demonstrated that the ratio of

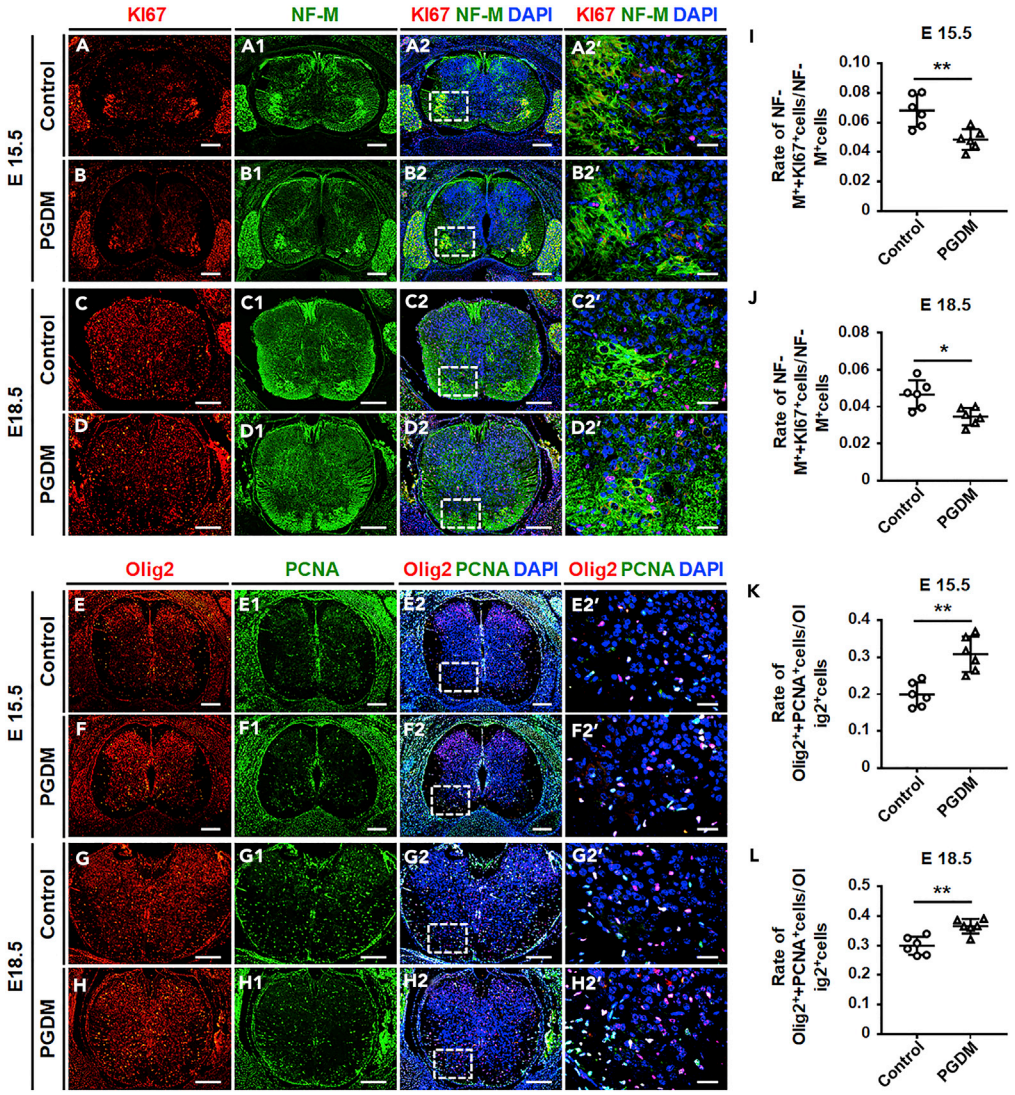

Figure 4. Determination of Cell Proliferation in the Fetal Trunk Neural Tubes of PGDM Mice

(A–D, A1–D1, A2–D2) Ki67 (red, A–D) and NF-M (green, A1–B1) double-immunofluorescent staining was performed on the transverse sections of E15.5 (A–A2 and B–B2) or E18.5 (C–C2 and D–D2) trunk neural tubes from control (A–A2 and C–C2) and PGDM (B–B2 and D–D2) groups, in which (A2–D2) were merged ones from Ki67 and NF-M staining, and then counterstained with DAPI.

(A2′–D2′) The high-magnification images from the sites indicated by the white squares in (A2–B2), respectively.

(E–H, E1–H1, and E2–H2) Olig2 (red, E–H) and PCNA (green, E1–H1) double-immunofluorescent staining was performed on the transverse sections of E15.5 (E–E2 and F–F2) or E18.5 (G–G2 and H–H2) trunk neural tubes from control (E–E2 and G–G2) and PGDM (F–F2 and H–H2) groups, in which (E2–H2) were merged ones from Olig2 and PCNA staining, and then counterstained with DAPI.

(E2′–H2′) The high-magnification images from the sites indicated by white squares in (E2–H2), respectively.

(I and J) Bar charts showing the rate comparisons of NF-M and Ki67 double-positive cells in total NF-M-positive cells on the transverse sections between E15.5 (I) or E18.5 (J) control embryos and PGDM embryos.

(K and L) Bar charts showing the rate comparisons of Oligo2 and PCNA double-positive cells in total Oligo2-positive cells on the transverse sections between E15.5 (K) or E18.5 (L) control embryos and PGDM embryos.

For (I–L), n = 6, t test, *$p < 0.05$, **$p < 0.01$. Data are represented as mean ± SEM. Scale bars, 500 μm in (A–H), (A1–H1), and (A2–H2) and 100 μm in (A2′–H2′).

NF-M + Ki67-positive cells in NF-M-positive cells from both E15.5 (Figure 4I) and E18.5 (Figure 4J) mouse embryos was significantly reduced in PGDM mice compared with controls. Double-immunofluorescent staining of Olig2 (glial cell marker) and PCNA (cell proliferation marker) was performed on the transverse

sections of neural tubes of E15.5 and E18.5 control and PGDM mouse embryos at trunk level (Figures 4E–4H, 4E1–4H1, and 4E2–4H2), and results demonstrated that the ratio of Olig2 + PCNA-positive cells in Olig2-positive cells from both E15.5 (Figure 4K) and E18.5 (Figure 4L) mouse embryos appreciably increased in PGDM mice compared with controls, indicating that neuronal proliferation was inhibited and glial cell proliferation was activated in diabetes mellitus mouse embryos.

PGDM Activates the Oxidative Stress and Nrf2 Signaling in Developing Mouse Neural Tubes, and Primary Culture of Neural Stem Cells and Differentiated Cells

To investigate whether or not oxidative stress is involved in the PGDM-induced maladjustment of neural stem cell development, we determined the various indicators for oxidative stress. First, we found that intracellular ROS production was much higher in hyperglycemia (25 mmol/L)-treated primary cultures of neural stem cells than in the controls (5.5 mmol/L) (Figures 5A and 5B). Second, we performed Nrf2 immunofluorescent staining on the primary culture of neural stem cells (Figures 5C and 5D) and differentiated cells (Figures 5F and 5G) to detect whether the Nrf2 was activated in the differentiation process of the neural stem cells in PGDM mice. The results showed a higher expression of Nrf2 in the hyperglycemia-treated cells compared with the controls (Figures 5E and 5H). Transmission electronic microcopy manifested that the numbers of mitochondria (indicated by red arrows) in neural stem cells of PGDM neural tubes were much more than the ones in controls (Figures 5I–5K). Both quantitative PCR (Figure 5L) and western blot (Figure 5M) displayed that expression of *Nrf2*, *HO1*, *SOD2*, *NQO1*, and *p62* was upregulated in PGDM mouse neural tubes when compared with the ones in controls, implying that oxidative stress and Nrf2 signaling are indeed activated in PGDM embryos, which in turn might influence or promote other signaling pathways.

Both CNTF and Nrf2 Can Affect Neural Stem Cell Differentiation in a High-Glucose Microenvironment

To further address the role of Nrf2 signaling in hyperglycemia-induced imbalance of neural precursors, we inspected the neuronal and glial cell markers in primary culture of differentiated cells in the absence or presence of CNTF when Nrf2 signaling was blocked with ML385 (Singh et al., 2016). Initially, Nrf2 and NF-M double-immunofluorescent staining demonstrated that hyperglycemia induced the proportional reduction of Nrf2-positive neurons in total NF-M-positive cells compared with control (Figures 6A–6C), whereas Nrf2 and GFAP double-immunofluorescent staining demonstrated that hyperglycemia induced the proportional increase of Nrf2-positive glial cells in total GFAP-positive cells compared with controls (Figures 6D–6F), implying the vital role of Nrf2 in neural differentiation under hyperglycemic conditions. Next, we found that addition of CNTF alone could elevate the neuron proportion (Figures 6G–6H″ and 6Q), whereas hyperglycemia (25 mmol/L) significantly suppressed the neuron proportion (Figures 6I–6I″ and 6Q); the combinational application of hyperglycemia and CNTF could rescue the neuron proportional decrease induced by hyperglycemia (Figures 6J–6J″ and 6Q), but the recovery of neuron proportion disappeared again (even reduced more than solo hyperglycemia treated) when Nrf2 signaling was blocked with ML385 (Figures 6K–6K″ and 6Q). For the glial cells, we manifested that the addition of CNTF only could inhibit the glial cell proportion (Figures 6L–6M′ and 6Q), whereas hyperglycemia (25 mmol/L) promoted the glial cell proportion (Figures 6N–6N′ and 6Q); the combinational application of hyperglycemia and CNTF could pull down the glial cell proportion increase induced by hyperglycemia (Figures 6O–6O′ and 6Q), but the increase of glial cell proportion occurred again when Nrf2 signaling was blocked with ML385 (Figures 6P–6P′ and 6Q). These data undoubtedly indicate the crucial role of both CNTF and Nrf2 signaling in regulating the differentiation of neural stem cells in PGDM. To explore the cross talk of Nrf2 signaling and CNTF expression, we performed the CNTF immunofluorescent staining on the primary culture of differentiated cells *in vitro* (Figure S5). The result showed that blocking Nrf2 with ML385 did not affect the CNTF expression level compared with the combined application of hyperglycemia and CNTF (Figures S5A–S5F), implying that there is not direct interaction between Nrf2 and CNTF expression (Figure S5G).

We then hypothesized that both Nrf2 and CNTF were regulating a key protein to affect the neural stem cell differentiation fate in a high-glucose microenvironment. To verify our hypothesis, we first checked the key molecules between Nrf2 signaling and neuropoietic cytokines using a bioinformatics approach (Figure 7A) (Paul et al., 2018). From the result, we could find that Nrf2 signaling and neuropoietic cytokines are closely associated with STAT3. Therefore, Nrf2 and p-STAT3 double-immunofluorescent staining was performed on primary culture of differentiated cells (Figures 7B–7F″). The results showed that hyperglycemia caused an increase in Nrf2 expression and ML385 could significantly reverse the hyperglycemia-induced Nrf2 increase; whereas CNTF addition promoted the expression of p-STAT3, hyperglycemia (25 mmol/L) inhibited p-STAT3 expression.

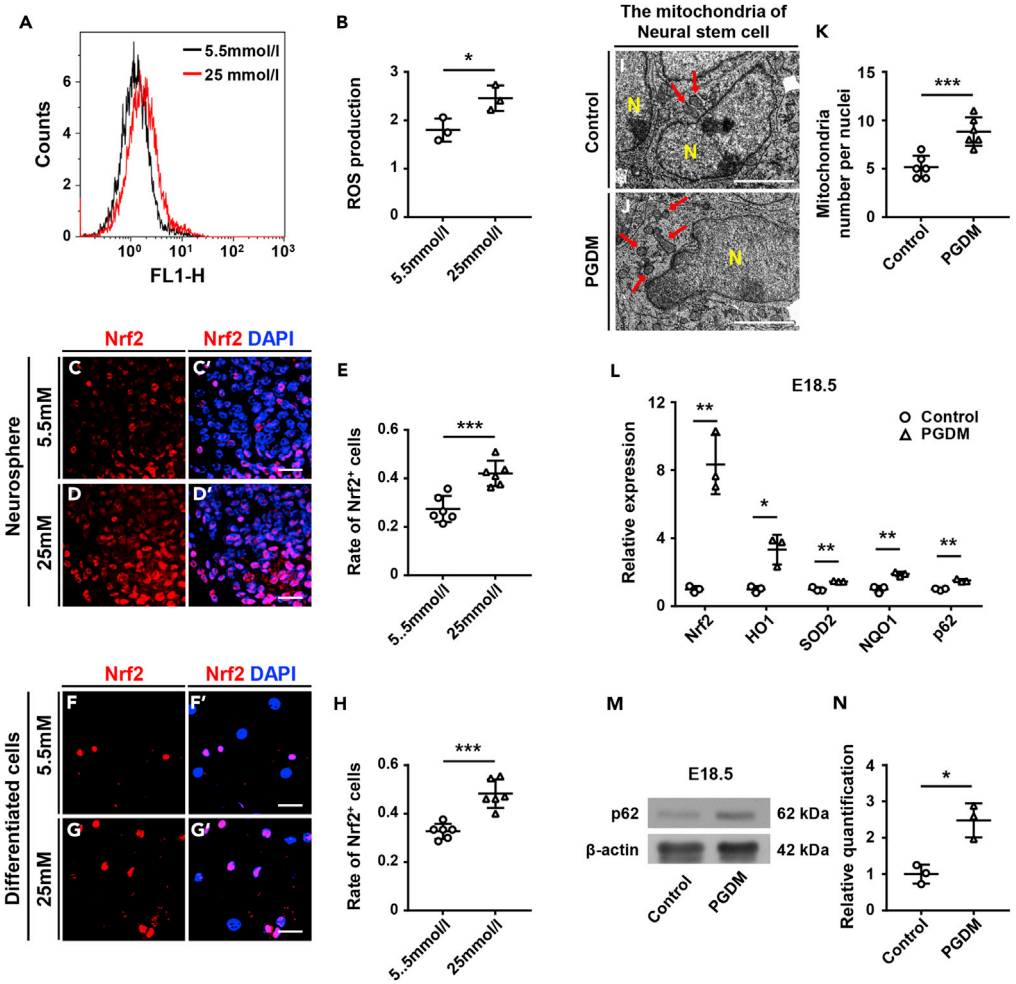

Figure 5. Assessing Hyperglycemia-Induced ROS and Oxidative Stress-Related Gene Expression Using *In Vivo* and *In Vitro* Models

(A and B) ROS level in cultured neurospheres exposed to 5.5 mmol/L and 25 mmol/L D-glucose was detected using flow cytofluorometry (A), and then ROS production in 5.5 mmol/L and 25 mmol/L D-glucose groups was quantitatively analyzed (B).

(C, D, C′, and D′) Nrf2 (red) immunofluorescent staining was performed on the neurospheres exposed to 5.5 mmol/L (C and C′) or 25 mmol/L D-glucose (D and D′), in which (C′ and D′) were counterstained with DAPI.

(F, G, F′, and G′) Nrf2 (red) immunofluorescent staining was performed on the differentiated cells exposed to 5.5 mmol/L (F and F′) or 25 mmol/L D-glucose (G and G′), in which (F′ and G′) were counterstained with DAPI.

(E and H) Bar charts showing the comparisons of Nrf2-positive cells in total cells labeled by DAPI between 5.5 mmol/L and 25 mmol/L D-glucose groups.

(I–K) The representative mitochondria images of neural progenitors taken by transmission electron microscope from the hippocampi of E15.5 control (I) and PGDM (J) embryos, in which mitochondria numbers were quantitatively analyzed (K). Arrows mark mitochondria.

(L) Quantitative PCR data showing the expression of *Nrf2*, *HO1*, *SOD2*, *NQO1*, and *p62* in E18.5 control and PGDM mouse embryos at mRNA level.

(M and N) Western blot data showing the expression of p62 in E18.5 control and PGDM mouse embryos at protein level (M), which was quantitatively analyzed (N).

For (B, L, and N), n = 3, for (E, H, and K), n = 6, t test, *$p < 0.05$, **$p < 0.01$, ***$p < 0.001$. Data are represented as mean ± SEM. Scale bars, 20 μm in (C, D, F, and G) and (C′, D′, F′, and G′) and 2 μm in (I and J).

A combination of CNTF and high glucose could counteract hyperglycemia-inhibited p-STAT3 expression, but p-STAT3 expression was suppressed again when Nrf2 signaling was blocked with ML385 (Figure 7G), which certainly indicates that STAT3 is the important downstream molecule of Nrf2 signaling in the process of regulating neural self-renewal and differentiation during embryonic neural development in PGDM.

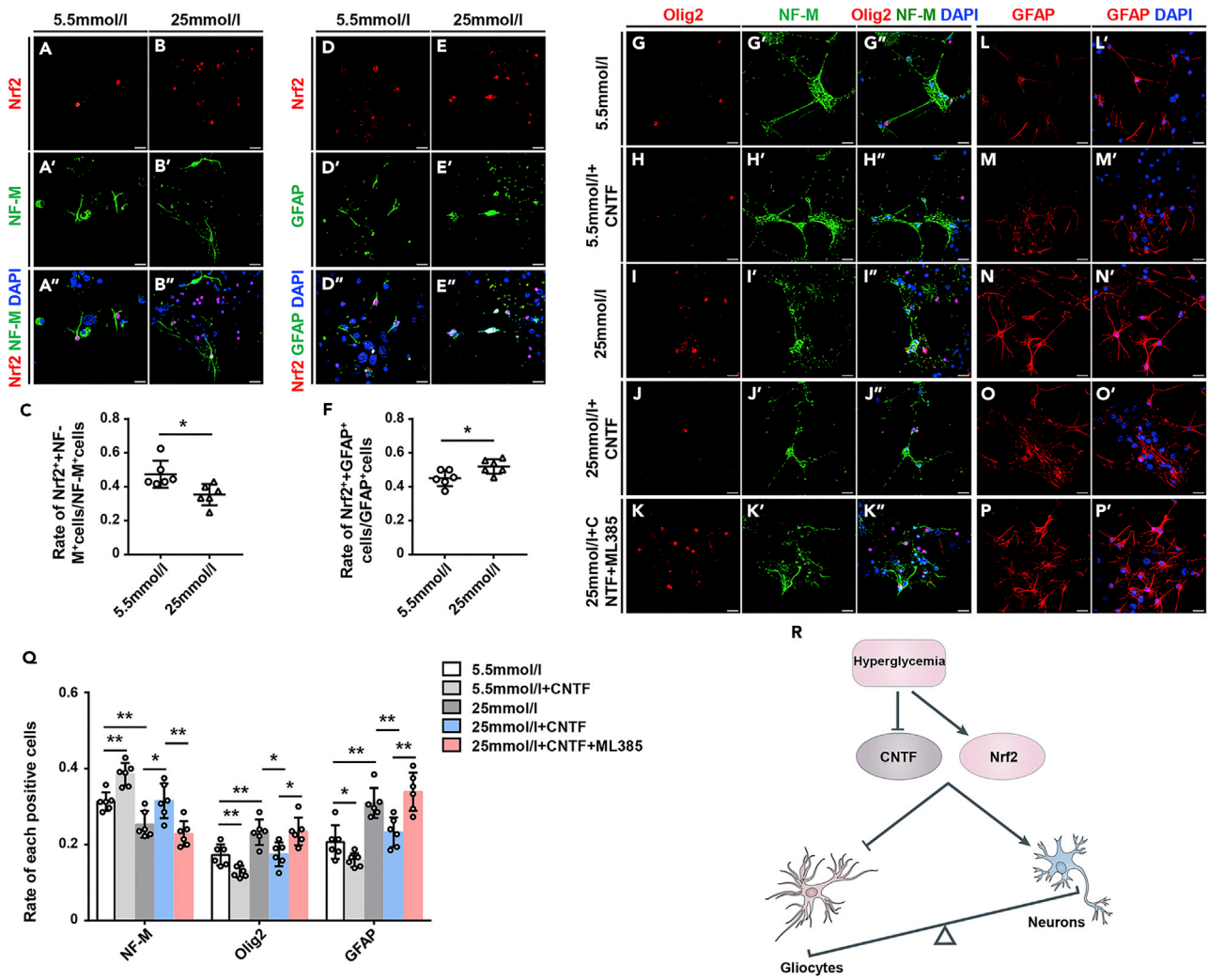

Figure 6. Determining Hyperglycemia-Induced Expression of Olig2, NF-M, and GFAP in Differentiated Cells when Adding CNTF or Blocking Nrf2

(A–A″ and B–B″) Nrf2 (red, A and B) and NF-M (green, A′ and B′) double-immunofluorescent staining was performed on differentiated cells under 5.5 mmol/L (A and A″) or 25 mmol/L D-glucose (B and B″), in which (A″ and B″) were merged ones counterstained with DAPI.

(C) Bar chart showing the rate comparisons of Nrf2 and NF-M double-positive cells in total Nrf2-positive cells.

(D–D″ and E–E″) Nrf2 (red, D and E) and GFAP (green, D′ and E′) double-immunofluorescent staining was performed on differentiated cells under 5.5 mmol/L (D–D″) or 25 mmol/L D-glucose (E–E″), in which (D″–E″) were merged ones counterstained with DAPI.

(F) Bar chart showing the rate comparisons of Nrf2 and GFAP double-positive cells in total Nrf2-positive cells.

(G–K, G′–K′, and G″–K″) Oligo2 (red, G–K) and NF-M (green, G′–K′) double-immunofluorescent staining was performed on differentiated cells under 5.5 mmol/L D-glucose (G–G″), 5.5 mmol/L D-glucose + CNTF (H–H″), 25 mmol/L D-glucose (I–I″), 25 mmol/L D-glucose + CNTF (J–J″), and 25 mmol/L D-glucose + CNTF + ML385 (K–K″), in which (G″ and K″) were merged ones counterstained with DAPI.

(L–P and L′–P′) GFAP (red, L–P) immunofluorescent staining was performed on differentiated cells exposed to 5.5 mmol/L D-glucose (L–L″), 5.5 mmol/L D-glucose + CNTF (M–M″), 25 mmol/L D-glucose (N–N″), 25 mmol/L D-glucose + CNTF (O–O″), 25 mmol/L D-glucose + CNTF + ML385 (P–P″), in which (L′–P′) were merged ones counterstained with DAPI.

(Q) Bar chart showing the rate comparisons of NF-M$^+$, Olig2$^+$, and GFAP$^+$ cells in total cells labeled by DAPI among various groups.

(R) A sketch illustrating the mechanism of how hyperglycemia affects neural differentiation.

For (C, F, and Q), n = 6, ANOVA, least significance difference, Student-Newman-Keuls, and t test, *p < 0.05, **p < 0.01. Data are represented as mean ± SEM. Scale bars, 20 μm in (A–A″), (B–B″), (D–D″), (E–E″), (G–P), (G′–P′), and (G″–K″). See also Figure S5.

DISCUSSION

In this study, we first confirmed the successful construction of a PGDM mouse model induced by STZ through the observation that blood glucose was kept at high level in PGDM mice after 3-day STZ injection (Figures S1A–S1C). PGDM noticeably increased the incidence rate of mouse fetal developmental

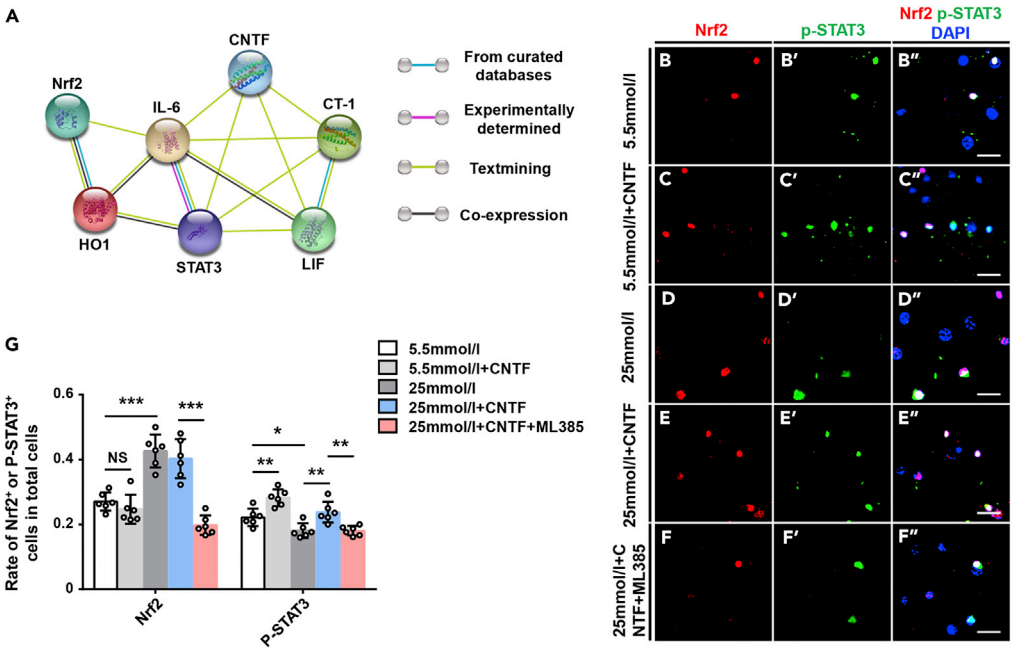

Figure 7. Determining Hyperglycemia-Induced Expression of Nrf2 and p-STAT3 in Differentiated Cells when Adding CNTF or Blocking Nrf2

(A) Bioinformatics analysis depicting the correlation between Nrf2/keap1 signaling and STAT3 signal transduction pathway were mapped with the STRING database to construct the protein-protein interaction (PPI) network.

(B–F, B′–F′, and B″–F″) Nrf2 (red, B–F) and p-STAT3 (green, B′–F′) double-immunofluorescent staining was performed on differentiated cells under 5.5 mmol/L D-glucose (B–B″), 5.5 mmol/L D-glucose + CNTF (C–C″), 25 mmol/L D-glucose (D–D″), 25 mmol/L D-glucose + CNTF (E–E″), and 25 mmol/L D-glucose + CNTF + ML385 (F–F″), in which (B″ and F″) were merged ones counterstained with DAPI.

(G) Bar chart showing the rate comparisons of $Nrf2^+$ and $p\text{-}STAT3^+$ cells in total cells labeled by DAPI among various groups. n = 6, ANOVA, least significance difference, Student-Newman-Keuls, and t test, *$p < 0.05$, **$p < 0.01$, ***$p < 0.001$. Data are represented as mean ± SEM. Scale bars, 20 μm in (B–F), (B′–F′), and (B″–F″).

anomalies, including encephalocele, spina bifida, anencephaly, and fetal resorption (Figures S1D–S1J). These phenotypes are mostly similar to the previous reports about neurodevelopmental defects in PGDM (Ornoy et al., 2015). It is noteworthy that most of the fetuses of pregnant diabetic mouse did not manifest any obvious morphological anomalies in the nervous system. However, even in this case, the possibility that PGDM negatively influences fetal neurodevelopment cannot be excluded because hyperglycemia's influence on neurogenesis was not so serious to cause the appearance of morphological manifestations. It is just based on this consideration that we chose the E15.5 or E18.5 PGDM embryos that appear either normal or show subtle anomalies for further immunohistochemistry experiments. It has been reported that maternal diabetes can delay neurogenesis from E8.5 to E10 (Xu et al., 2013), and here we mainly focus on the effect of hyperglycemia on cell fate decision of neural stem cells at later gestation stage in this study, so that we chose E12.5, E15.5, and E18.5 as time points. In the subsequent experiments, we demonstrated that the differentiation of neural stem cells toward NF-M- or Tuj1-labeled neuronal linkage was inhibited, but the differentiation toward Olig2 or GFAP-labeled glial cell linkage was promoted in both PGDM mouse embryos and *in vitro* model (Figures 1 and S2–S4), which is comparable to the report about diabetes-impaired neurogenesis reflected in neuronal proliferation, differentiation, and cell survival (Dorsemans et al., 2017).

In tracking the possible cause of PGDM-induced phenotypes, we found a downregulation of CNTF and upregulation of CT-1 and LIF in E15.5 PGDM mouse neural tubes compared with control mice (Figure 2). As we know, all CNTF, LIF, and CT-1 belong to the neuropoietic family (Bauer et al., 2007). CNTF is well known to be involved in normal nervous system development during embryogenesis, and it sequesters in adult glial cells and becomes activated or secreted again as a cytokine during injury (Bauer et al., 2007). It has been reported that CNTF inhibited lineage restriction of neural stem cells to glial progenitors, resulting in

enhanced expansion of stem cell number (Shimazaki et al., 2001). CNTF administration can stimulate neurogenesis in the adult hippocampus and hypothalamus (Emsley and Hagg, 2003; Kokoeva et al., 2005). LIF is considered to reduce neurogenesis of neural stem cells (Bauer and Patterson, 2006) and mediated astrogliogenesis in mouse embryos later than E15 (Barnabe-Heider et al., 2005). CT-1 was generated in newly born neurons and controlled multipotent cortical precursors to differentiate into astrocytes, a neural feedback by an autocrine or paracrine mechanism (Barnabe-Heider et al., 2005).

Therefore, the up- and downregulation of CT-1 and CNTF expression in the PGDM mouse could contribute to the promoted developmental switch toward gliogenesis during embryonic neurogenesis. Still, the spatiotemporal coordination of the neuropoietic cytokine family rather than one single alteration is indispensably emphasized, which is partially due to the developmental time difference between neurogenesis and gliogenesis. Our result suggests that the self-renewal of neural stem cells was suppressed by hyperglycemia (Figure 3). A neurosphere assay was employed to verify the above observation because it (Figure S4) can offer a uniform *in vitro* platform of neural stem cells to determine self-renewal and differentiation of neural stem cells (Reynolds and Weiss, 1992). Actually, the fact that hyperglycemia inhibited neural stem cell proliferation was confirmed in the *in vitro* neurosphere assay, and addition of exogenous CNTF could partially rescue the cell proliferation inhibition induced by hyperglycemia, indicating again the key role of CNTF in neural stem cell self-renewal in PGDM mice (Figures 3S–3X). In addition, we also discovered that the differentiated neuronal cell proliferation in mouse neural tubes was repressed, and differentiated glial cell proliferation in mouse neural tubes was promoted by PGDM (Figure 4), which suggests that sensitivity toward hyperglycemia was different between differentiated neuronal cells and differentiated glial cells.

Oxidative imbalance has negative effects on neural stem cell self-renewal and differentiation by influencing the expression of important gene transcription factors during cell proliferation, migration, differentiation, and apoptosis (Dennery, 2007). Our study also indicated that hyperglycemia-induced oxidative stress directly or indirectly exerts effects on the embryonic neural stem or progenitor cells (Figure 5). p62 interacts with the Nrf2-binding site on Keap1, and overproduction of p62 competes with the interaction between Nrf2 and Keap1, resulting in stabilization of Nrf2 and transcriptional activation of Nrf2 target genes (Komatsu et al., 2010). In this study, Nrf2 signaling specific activity and expression of p62 were significantly enhanced in PGDM or hyperglycemia groups, suggesting that Nrf2 plays a crucial role against the oxidative stress in this process. To confirm the prediction, we established the co-localization expression of neuron marker (NF-M) and Nrf2 using immunofluorescent staining in the primary culture of neural stem cells, and hyperglycemia inhibited Nrf2-positive neurons rather than glial cells (Figures 6A–6E). Fascinatingly, blocking Nrf2 transcription activity with ML385 could inhibit CNTF-promoted neuronal differentiation linkage, but re-raised CNTF-inhibited glial cell differentiation linkage in neurosphere assay (Figures 6G–6Q), implying that Nrf2-modulated oxidative stress is involved in neural differentiation from neural stem or progenitor cells. There was no alteration of CNTF expression when Nrf2 transcription activity was blocked (Figures S5A–S5F), indicating that Nrf2 is directly involved in twisting the developmental switch from neurogenesis to gliogenesis instead of influencing CNTF indirectly in the presence of hyperglycemia (Figures 6R and S5G). Bioinformatics also provides the correlation between Nrf2/keap1 signaling and the STAT3 signal transduction pathway (Figure 7A). One more robust evidence to support the view above is that addition of CNTF could promote p-STAT3 signaling in the presence of hyperglycemia, but blocking Nrf2 transcription activity with its inhibitor would lead to the reduction of the p-STAT3 signal transduction pathway (Figures 7B–7G), by which neuropoietic cytokines like CNTF control neural stem cell renewal and differentiation.

In sum, this study revealed the impact of PGDM on neural stem cell self-renewal and differentiation and the corresponding mechanisms responsible for these effects. We demonstrated that PGDM or hyperglycemia could inhibit neural stem cell self-renewal and twist the developmental switch from neurogenesis into gliogenesis during early embryo development. In this process, neuropoietic cytokine, CNTF, has a very important impact on the regulation of neural stem cell self-renewal and differentiation. Another vital mediator involved is Nrf2 signaling, which has been verified to be independently implicated in the regulation of cell survival and differentiation during neural development. At last, we proved that CNTF and Nrf2 are coordinately involved in regulating differentiation of neural stem cells through p-STAT3. This undoubtedly suggests an avenue for confronting PGDM-induced neurodevelopmental defects, although more precise cellular and molecular biological experiments might be required to further solidify the conclusion.

Limitations of the Study

Although this study revealed that PGDM suppressed the self-renewal ability of neural progenitor cells and induced an imbalance between neurogenesis and gliogenesis, we did not address whether or not these phenotypes could result in changes neurological function, because neurofunctional assessments have not yet been performed. In addition, the development of the nervous system is complex and regulated by a series of more broadly signaling pathways, therefore, more precise cellular and molecular mechanisms need to be explored in future studies.

METHODS

All methods can be found in the accompanying Transparent Methods supplemental file.

DATA AND CODE AVAILABILITY

The data that support the findings of this study are available from the corresponding author upon reasonable request.

SUPPLEMENTAL INFORMATION

Supplemental Information can be found online at https://doi.org/10.1016/j.isci.2019.07.038.

ACKNOWLEDGMENTS

This study was supported by NSFC grant (81741083, 81801492, 31771331, 81741016), Guangdong Natural Science Foundation (2018A030310598, 2016A030311044), Science and Technology Planning Project of Guangdong Province (2017A050506029, 2017A020214015, 2016B030229002), Special Funds for the Cultivation of Guangdong College Students' Scientific and Technological Innovation (pdjh2018b0064, pdjh2019b0066), National Innovation and Entrepreneurship Training Program for Undergraduate (201810559028), Science and Technology Program of Guangzhou (201710010054), and Cultivation Fund of First Affiliated Hospital of Jinan University.

AUTHOR CONTRIBUTIONS

Z.-P.S., G.W., X.Y., and G.-S.L. were responsible for the overall experimental design, Z.-P.S. and G.W. performed the majority of the experiments, with S.-S.H. and Y.J. providing assistance. Y.-X.H. and M.-Y.H. performed part of *in vitro* experiments, with G.-S.L. supervising these studies. X.Y. and G.-S.L. secured funding. X.Y. wrote the manuscript, and B.B.-S. provided feedback.

DECLARATION OF INTERESTS

The authors declare no competing interests.

Received: January 16, 2019
Revised: June 4, 2019
Accepted: July 24, 2019
Published: September 27, 2019

REFERENCES

Adler, R., Landa, K.B., Manthorpe, M., and Varon, S. (1979). Cholinergic neuronotrophic factors: intraocular distribution of trophic activity for ciliary neurons. Science *204*, 1434–1436.

Barnabe-Heider, F., Wasylnka, J.A., Fernandes, K.J., Porsche, C., Sendtner, M., Kaplan, D.R., and Miller, F.D. (2005). Evidence that embryonic neurons regulate the onset of cortical gliogenesis via cardiotrophin-1. Neuron *48*, 253–265.

Bauer, S., Kerr, B.J., and Patterson, P.H. (2007). The neuropoietic cytokine family in development, plasticity, disease and injury. Nat. Rev. Neurosci. *8*, 221–232.

Bauer, S., and Patterson, P.H. (2006). Leukemia inhibitory factor promotes neural stem cell self-renewal in the adult brain. J. Neurosci. *26*, 12089–12099.

Canning, C.A., Lee, L., Luo, S.X., Graham, A., and Jones, C.M. (2008). Neural tube derived Wnt signals cooperate with FGF signaling in the formation and differentiation of the trigeminal placodes. Neural Dev. *3*, 35.

Correa, A., Gilboa, S.M., Besser, L.M., Botto, L.D., Moore, C.A., Hobbs, C.A., Cleves, M.A., Riehle-Colarusso, T.J., Waller, D.K., and Reece, E.A. (2008). Diabetes mellitus and birth defects. Am. J. obstetrics Gynecol. *199*, 237.e1–237.e9.

Corrigan, N., Brazil, D.P., and McAuliffe, F. (2009). Fetal cardiac effects of maternal hyperglycemia during pregnancy. Birth Defects Res. A. Clin. Mol. Teratol. *85*, 523–530.

De Robertis, E.M., and Kuroda, H. (2004). Dorsal-ventral patterning and neural induction in Xenopus embryos. Annu. Rev. Cell Dev. Biol. *20*, 285–308.

Dennery, P.A. (2007). Effects of oxidative stress on embryonic development. Birth Defects Res. C Embryo Today *81*, 155–162.

Dorsemans, A.C., Couret, D., Hoarau, A., Meilhac, O., Lefebvre d'Hellencourt, C., and

Diotel, N. (2017). Diabetes, adult neurogenesis and brain remodeling: new insights from rodent and zebrafish models. Neurogenesis *4*, e1281862.

Du, Z.W., and Zhang, S.C. (2004). Neural differentiation from embryonic stem cells: which way? Stem cells Dev. *13*, 372–381.

Emsley, J.G., and Hagg, T. (2003). Endogenous and exogenous ciliary neurotrophic factor enhances forebrain neurogenesis in adult mice. Exp. Neurol. *183*, 298–310.

Giordano, F.J. (2005). Oxygen, oxidative stress, hypoxia, and heart failure. J. Clin. Invest. *115*, 500–508.

Han, S.S., Wang, G., Jin, Y., Ma, Z.L., Jia, W.J., Wu, X., Wang, X.Y., He, M.Y., Cheng, X., Li, W.J., et al. (2015). Investigating the mechanism of hyperglycemia-induced fetal cardiac hypertrophy. PLoS One *10*, e0139141.

Itoh, K., Mimura, J., and Yamamoto, M. (2010). Discovery of the negative regulator of Nrf2, Keap1: a historical overview. Antioxid. Redox signaling *13*, 1665–1678.

Jaiswal, A.K. (2004). Nrf2 signaling in coordinated activation of antioxidant gene expression. Free Radic. Biol. Med. *36*, 1199–1207.

Jin, Y., Wang, G., Han, S.S., He, M.Y., Cheng, X., Ma, Z.L., Wu, X., Yang, X., and Liu, G.S. (2016). Effects of oxidative stress on hyperglycaemia-induced brain malformations in a diabetes mouse model. Exp. cell Res. *347*, 201–211.

Karbownik, M., and Lewinski, A. (2003). The role of oxidative stress in physiological and pathological processes in the thyroid gland; possible involvement in pineal-thyroid interactions. Neuro Endocrinol. Lett. *24*, 293–303.

Kokoeva, M.V., Yin, H., and Flier, J.S. (2005). Neurogenesis in the hypothalamus of adult mice: potential role in energy balance. Science *310*, 679–683.

Komatsu, M., Kurokawa, H., Waguri, S., Taguchi, K., Kobayashi, A., Ichimura, Y., Sou, Y.S., Ueno, I., Sakamoto, A., Tong, K.I., et al. (2010). The selective autophagy substrate p62 activates the stress responsive transcription factor Nrf2 through inactivation of Keap1. Nat. Cell Biol. *12*, 213–223.

Macintosh, M.C., Fleming, K.M., Bailey, J.A., Doyle, P., Modder, J., Acolet, D., Golightly, S., and Miller, A. (2006). Perinatal mortality and congenital anomalies in babies of women with type 1 or type 2 diabetes in England, Wales, and Northern Ireland: population based study. BMJ *333*, 177.

Murdoch, C.E., Zhang, M., Cave, A.C., and Shah, A.M. (2006). NADPH oxidase-dependent redox signalling in cardiac hypertrophy, remodelling and failure. Cardiovasc. Res. *71*, 208–215.

Ornoy, A., Reece, E.A., Pavlinkova, G., Kappen, C., and Miller, R.K. (2015). Effect of maternal diabetes on the embryo, fetus, and children: congenital anomalies, genetic and epigenetic changes and developmental outcomes. Birth Defects Res. C Embryo Today *105*, 53–72.

Paul, S., Gangwar, A., Bhargava, K., and Ahmad, Y. (2018). STAT3-RXR-Nrf2 activates systemic redox and energy homeostasis upon steep decline in pO2 gradient. Redox Biol. *14*, 423–438.

Regan, C.M. (1988). Neuronal and glial markers of the central nervous system. Experientia *44*, 695–697.

Reynolds, B.A., and Weiss, S. (1992). Generation of neurons and astrocytes from isolated cells of the adult mammalian central nervous system. Science *255*, 1707–1710.

Rice, D., and Barone, S., Jr. (2000). Critical periods of vulnerability for the developing nervous system: evidence from humans and animal models. Environ. Health Perspect. *108* (*Suppl 3*), 511–533.

Rodier, P.M. (1994). Vulnerable periods and processes during central nervous system development. Environ. Health Perspect. *102* (*Suppl 2*), 121–124.

Rushmore, T.H., and Pickett, C.B. (1990). Transcriptional regulation of the rat glutathione S-transferase Ya subunit gene. Characterization of a xenobiotic-responsive element controlling inducible expression by phenolic antioxidants. J. Biol. Chem. *265*, 14648–14653.

Sawyer, D.B., Siwik, D.A., Xiao, L., Pimentel, D.R., Singh, K., and Colucci, W.S. (2002). Role of oxidative stress in myocardial hypertrophy and failure. J. Mol. Cell Cardiol. *34*, 379–388.

Shimazaki, T., Shingo, T., and Weiss, S. (2001). The ciliary neurotrophic factor/leukemia inhibitory factor/gp130 receptor complex operates in the maintenance of mammalian forebrain neural stem cells. J. Neurosci. *21*, 7642.

Singal, P.K., Bello-Klein, A., Farahmand, F., and Sandhawalia, V. (2001). Oxidative stress and functional deficit in diabetic cardiomyopathy. Adv. Exp. Med. Biol. *498*, 213–220.

Singh, A., Venkannagari, S., Oh, K.H., Zhang, Y.Q., Rohde, J.M., Liu, L., Nimmagadda, S., Sudini, K., Brimacombe, K.R., Gajghate, S., et al. (2016). Small molecule inhibitor of NRF2 selectively intervenes therapeutic resistance in KEAP1-deficient NSCLC tumors. ACS Chem. Biol. *11*, 3214–3225.

Timmer, J.R., Wang, C., and Niswander, L. (2002). BMP signaling patterns the dorsal and intermediate neural tube via regulation of homeobox and helix-loop-helix transcription factors. Development *129*, 2459–2472.

Valko, M., Leibfritz, D., Moncol, J., Cronin, M.T., Mazur, M., and Telser, J. (2007). Free radicals and antioxidants in normal physiological functions and human disease. Int. J. Biochem. Cell Biol. *39*, 44–84.

Varon, S., Manthorpe, M., and Adler, R. (1979). Cholinergic neuronotrophic factors: I. Survival, neurite outgrowth and choline acetyltransferase activity in monolayer cultures from chick embryo ciliary ganglia. Brain Res. *173*, 29–45.

Wells, P.G., McCallum, G.P., Chen, C.S., Henderson, J.T., Lee, C.J., Perstin, J., Preston, T.J., Wiley, M.J., and Wong, A.W. (2009). Oxidative stress in developmental origins of disease: teratogenesis, neurodevelopmental deficits, and cancer. Toxicol. Sci. *108*, 4–18.

Wilson, L., and Maden, M. (2005). The mechanisms of dorsoventral patterning in the vertebrate neural tube. Dev. Biol. *282*, 1–13.

Xu, C., Li, X., Wang, F., Weng, H., and Yang, P. (2013). Trehalose prevents neural tube defects by correcting maternal diabetes-suppressed autophagy and neurogenesis. Am. J. Physiol. Endocrinol. Metab. *305*, E667–E678.

Zangen, S.W., Yaffe, P., Shechtman, S., Zangen, D.H., and Ornoy, A. (2002). The role of reactive oxygen species in diabetes-induced anomalies in embryos of Cohen diabetic rats. Int. J. Exp. Diabetes Res. *3*, 247–255.

Zhang, D.D. (2006). Mechanistic studies of the Nrf2-Keap1 signaling pathway. Drug Metab. Rev. *38*, 769–789.

Zirra, A., Wiethoff, S., and Patani, R. (2016). Neural conversion and patterning of human pluripotent stem cells: a developmental perspective. Stem Cells Int. *2016*, 8291260.

ISCI, Volume *19*

Supplemental Information

CNTF and Nrf2 Are Coordinately Involved in Regulating Self-Renewal and Differentiation of Neural Stem Cell during Embryonic Development

Zhen-Peng Si, Guang Wang, Sha-Sha Han, Ya Jin, Yu-Xuan Hu, Mei-Yao He, Beate Brand-Saberi, Xuesong Yang, and Guo-Sheng Liu

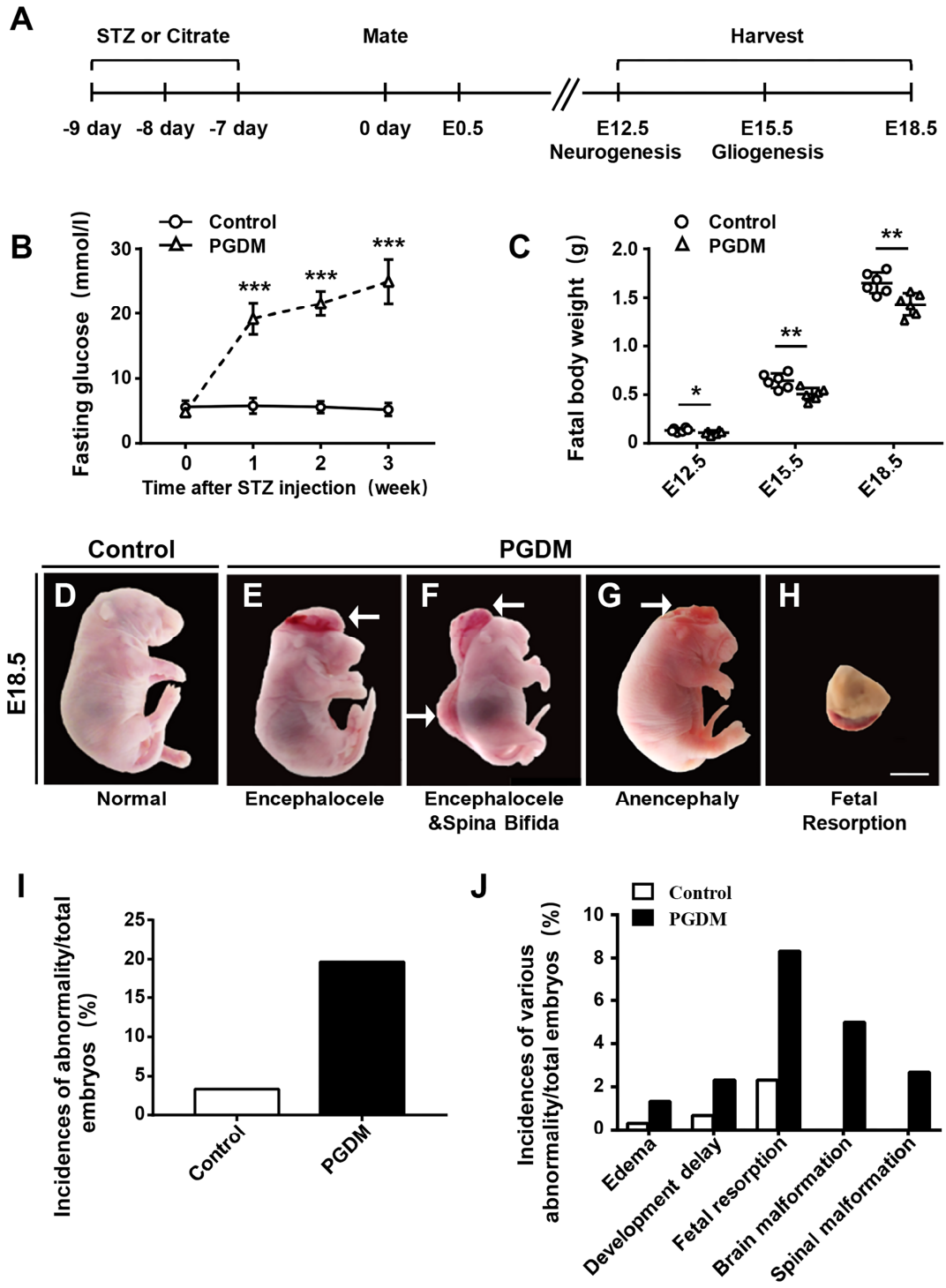

Figure S1. Detecting blood glucose and general condition of fetal development in pregnant STZ-induced PGDM mice, related to Figure 1.

A: A sketch illustrating when the STZ/citrate was injected before mating and when the fetuses were

harvested after pregnancy. **B-C**: The detection of mouse maternal glucose blood in week 0-3 weeks (B), and the harvested fetal weights in E12,5, E15.5, E18.5, respectively, in control and PGDM groups. **D-H**: The representative E18.5 fetus from control (D) and PGDM (E-H) group, in which there were different phenotypes of fetuses of maternal PGDM mice (F-H). **I-J**: Bar charts showing the percentages of abnormal embryos (I), the percentages of each kind of abnormal embryos (J), respectively, in control and PGDM groups. For (B-C), n=6, *t* test, **p* < 0.05, ***p* < 0.01, ****p* < 0.001. Data are represented as mean ± SEM. Scale bars: 50 μm in D-H.

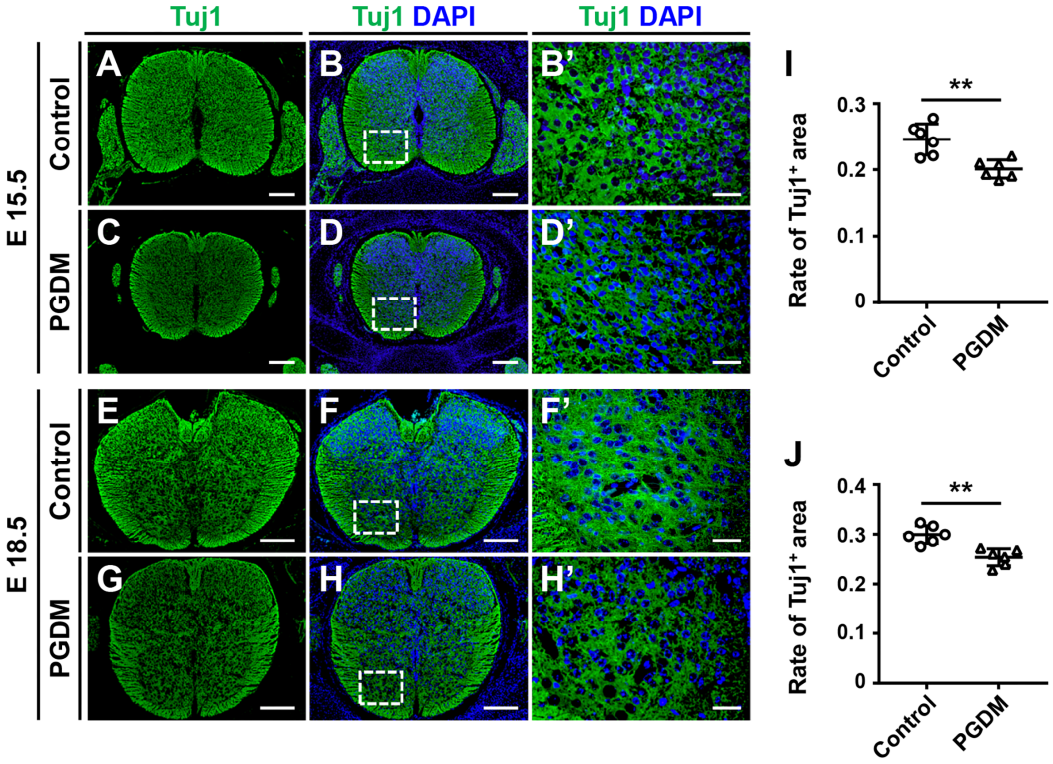

Figure S2. Determination the expression of Tuj1 in the fetal trunk neural tubes of PGDM mice, related to Figure 1.

A-H: Tuj1 immunofluorescent staining was performed on the transverse sections of E15.5 (A-D) or E15.5 (E-H) trunk neural tubes respectively from control (A-B, E-F) and PGDM (C-D, G-H) groups, in which B, D, F, H images were counterstained with DAPI. **B', D', F', H'**: The high magnification images from the sites indicated by white squares in B, D, F, H. **I-J**: Bar charts showing the rate comparisons of Tuj1+ areas of E15.5 mice (I) or E18.5 mice (J) respectively between control and PGDM group. n=6, *t* test, **p < 0.01. Data are represented as mean ± SEM. Scale bars: 500 μm in A-H, 100 μm in B', D', F', H'.

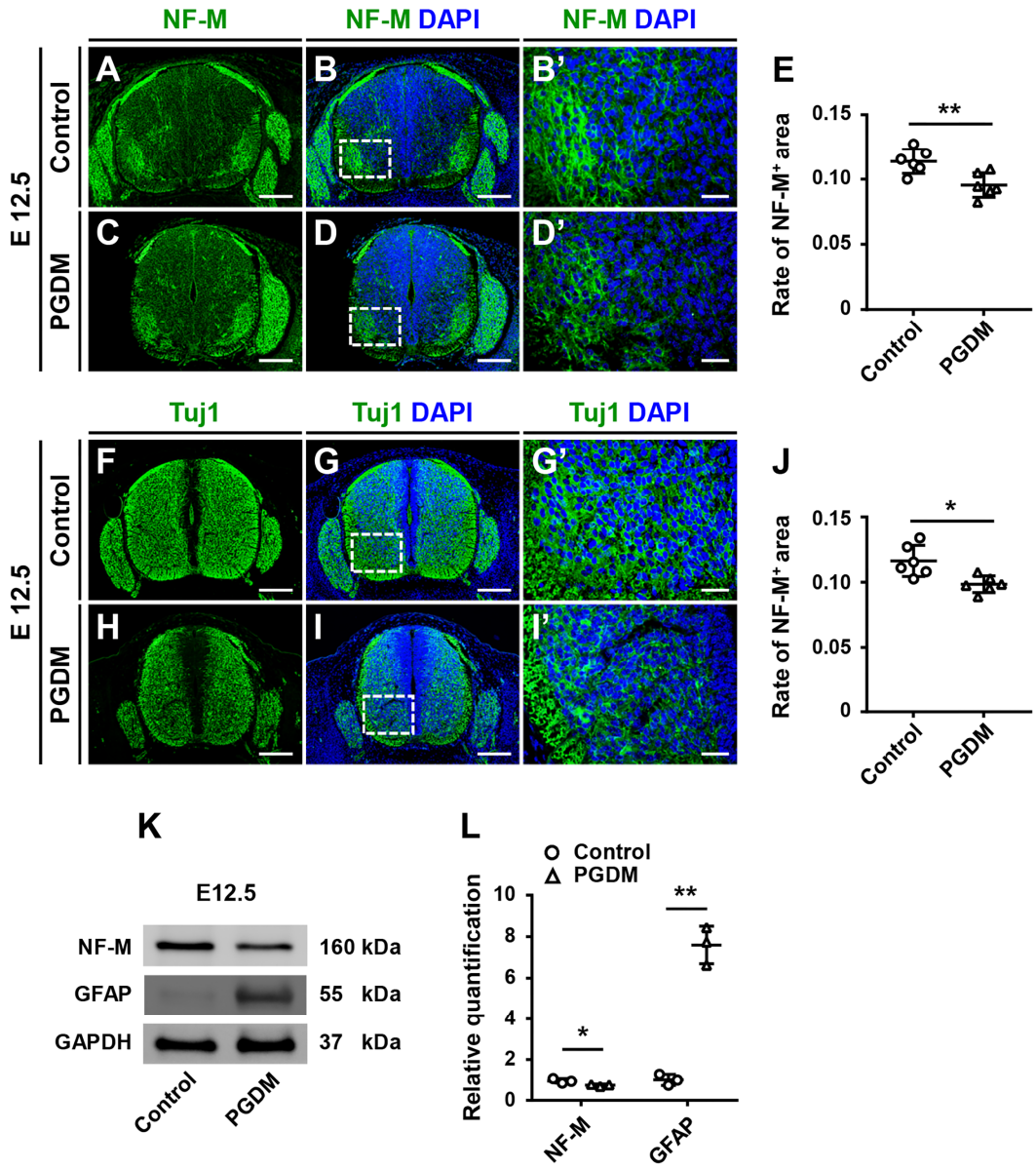

Figure S3. Determination of crucial gene expression of neuronal differentiation in the fetal trunk neural tubes of E12.5 PGDM mice, related to Figure 1.

A-D, F-I: NF-M (green, A-D) or Tuj1 (green, F-I) immunofluorescent staining was performed on the transverse sections of E12.5 trunk neural tubes respectively from control (A-B, F-G) or PGDM (C-D, H-I) groups, in which B, D, G, I images were counterstained with DAPI. **B', D', G', I'**: The high magnification images from the sites indicated by white squares in B, D, G, I. **E, J**: Bar charts showing the rate comparisons of NF-M$^+$ areas (E), Tuj1$^+$ areas (J) between control and PGDM group. **K-L**: Western blot data showing the expression of NF-M and GFAP in E12.5 control and PGDM mouse embryos at protein level (K), which was quantitatively analyzed (L). For (E) and (J), n=6, for (L), n=3, *t* test, **p* < 0.05, ***p* < 0.01. Data are represented as mean ± SEM. Scale bars:

500 μm in A-I and 100 μm in B', D', G', I'.

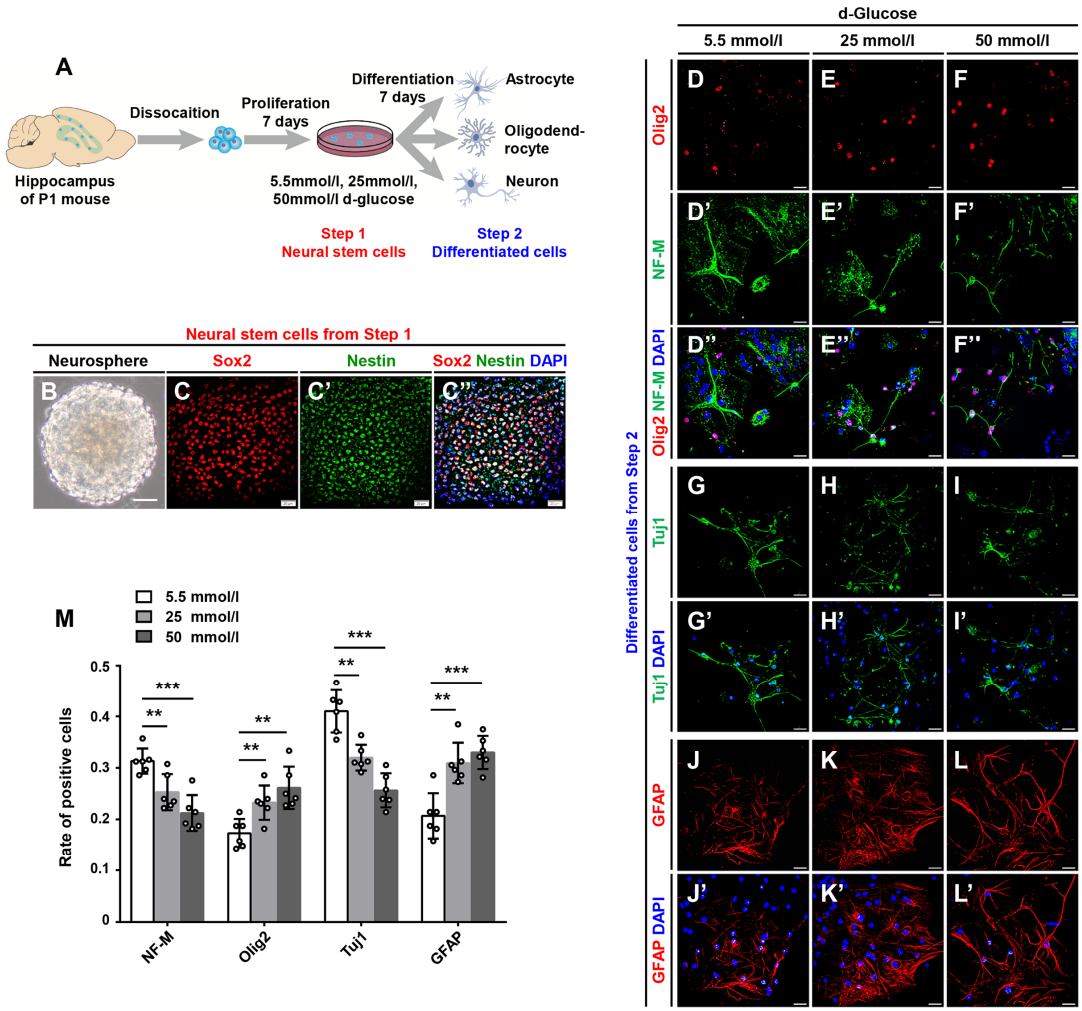

Figure S4. Assessing the differentiation fate of neural stem cells from primary culture under the high concentration of d-glucose, related to Figure 1.

A: A Sketch illustrating when/where the neural progenitor cells were isolated from P1 mice and how the d-glucose was administrated in primary culture. **B**: A typical bright-field image of primary cultured neurospheres (B). **C-C''**: Sox2 (red, C) and Nestin (green, C') double-immunofluorescent staining was performed on primary cultured neurospheres under 5.5 mmol/l d-glucose, in which C'' image was counterstained with DAPI. **D-F, D'-F', D''-F''**: Olig2 (red, D-F) and NF-M (green, D'-F') double-immunofluorescent staining was performed on differentiated cells under 5.5 mmol/l (D, D'), 25 mmol/l (E, E'), 50 mmol/l (F, F') d-glucose, in which D''-F'' images were merged ones counterstained with DAPI. **G-I, G'-I'**: Tuj1 (green, G-I) immunofluorescent staining was performed on differentiated cells under 5.5 mmol/l (G, G'), 25 mmol/l (H, H'), 50 mmol/l (I, I') d-glucose, in which G'-I' images were counterstained with DAPI. **J-L, J'-L'**: GFAP (red, G-I) immunofluorescent staining was performed on differentiated cells under 5.5 mmol/l (J, J'), 25 mmol/l (K, K'), 50 mmol/l

(L, L') d-glucose, in which J'-L' images were counterstained with DAPI. **M**: Bar chart showing the comparisons of NF-M, Olig2, Tuj1, GFAP positive cells in total cells labeled by DAPI in the differentiated cells treated with 5.5 mmol/l, 25 mmol/l, 50 mmol/l d-glucose. n=6, ANOVA, LSD, SNK and *t* test, **p < 0.01, ***p < 0.001. Data are represented as mean ± SEM. Scale bars: 50 μm in B and 20 μm in C-J, C'-J'.

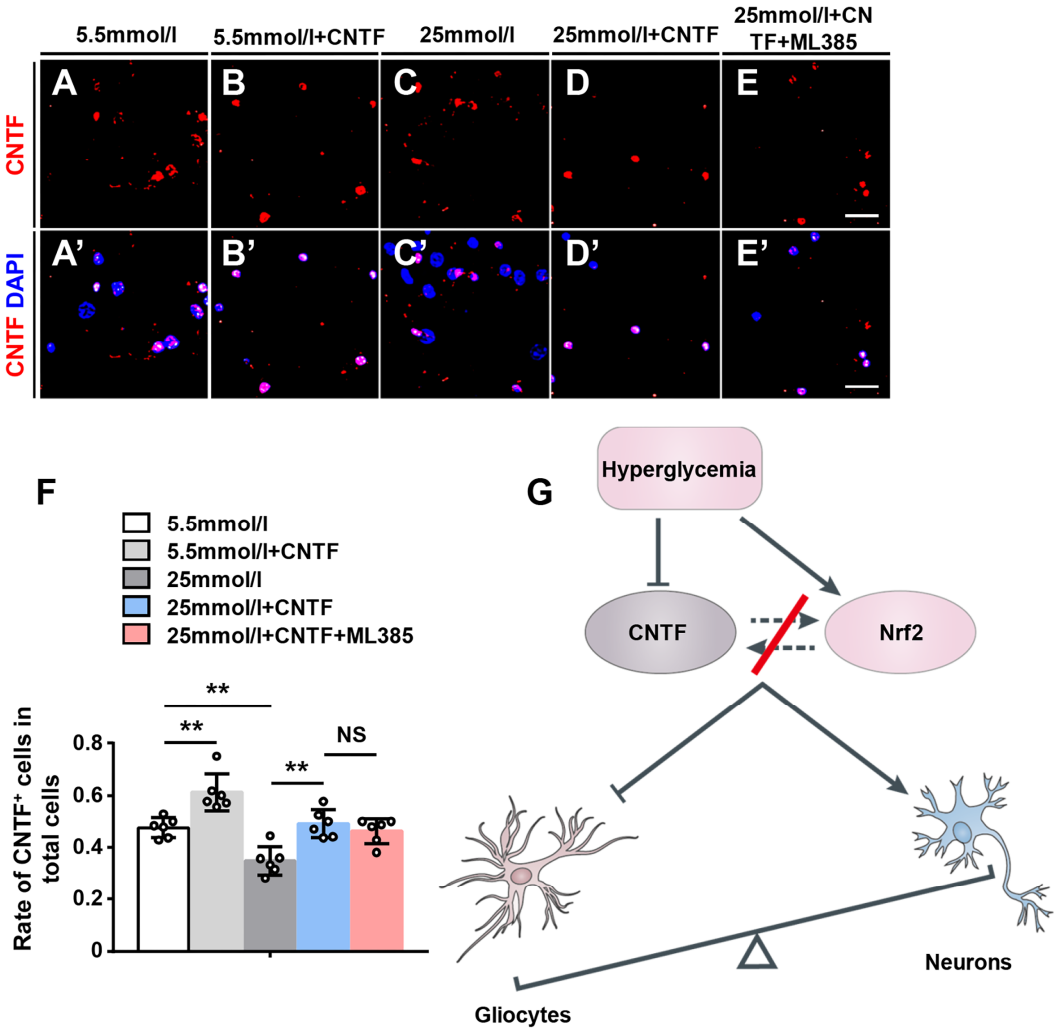

Figure S5. Determining hyperglycemia-induced expression of CNTF in differentiated cells when adding CNTF or blocking Nrf2, related to Figure 6.

A-E, A'-E': CNTF (red, A-E) immunofluorescent staining was performed on differentiated cells exposed to 5.5 mmol/l d-glucose (A-A'), 5.5 mmol/l d-glucose + CNTF (B-B'), 25 mmol/l d-glucose (C-C'), 25 mmol/l d-glucose + CNTF (D-D'), 25 mmol/l d-glucose + CNTF + ML385 (E-E'), in which A'-E' images were merged ones counterstained with DAPI. **F**: Bar charts showing the rate comparisons of $CNTF^+$ cells in total cells labeled by DAPI among various groups. **G**: A model illustrating the relationship between CNTF and Nrf2. n=6, *t* test, $^{**}p < 0.01$. Data are represented as mean ± SEM. Scale bars: 20 μm in A-E, A'-E'.

Transparent Methods

Reagents and antibodies

All antibodies are at concentration of 1 μg/ml and used at 1:200 dilution for immunofluorescent staining and 1:1,000 dilution for western blot unless otherwise stated. Anti-GFAP (ab7260), anti-Tuj1 (ab78078), anti-Ki67 (ab15580), anti-Sox2 (ab171380), anti-PCNA (ab29), anti-CNTF (ab46172), anti-LIF (ab113262), anti-Nestin (ab6142) and anti-GAPDH (ab181602) from Abcam; Santa Cruz; anti-Olig2 (P219454) and anti-NF-M (13-0700) from Invitrogen; anti-Nrf2 (SC-722) from Santa Cruz; anti-CT-1 (bs-2534R) from Bioss; anti-p-STAT3 (4113) from Cell Signaling Technology; anti-p62 (AP2183B) from Abgent; anti-β-actin (60008-1) from Proteintech.

Experimental Animals

The Kunming mice used in this study were obtained from Huafukang bioscience company (Beijing, China). Eight-week old female mice were used to induce diabetes mellitus by injecting STZ (Sigma, MO, USA) dissolved in 0.01 mol/l citrate buffer at a pH of 4.5 and a dose of 75 mg/kg body weight for three consecutive days. Blood glucose levels were measured 7 days after STZ injection by Roche Accu-Chek Aviva Blood Glucose System (Roche, USA). Diabetes mellitus was defined as a fasting blood glucose level greater than 288 mg/dl (16 mmol/l) [1, 2]. Control mice were maintained euglycemic prior to and during pregnancy (4–8 mmol/l). Two female mice were housed with one normal male mouse overnight in a cage. The day that vaginal plugs were observed was designated as embryonic day 0.5 (E0.5). During pregnancy, blood glucose levels were monitored every 6 days. At E12.5, E15.5 and E18.5, the fetuses were dissected by caesarean section after the pregnant mice were anaesthetized by injecting pentobarbital (150 mg/kg body weight). E12.5 and E15.5, corresponding to 6 weeks and 8 weeks of human fetal development stage, were chose in our study, because the two time points represent key stages of fetal neurogenesis and gliogenesis respectively. The experiments were performed in triplicates for the three embryonic days, with 24 mice assigned to control and PGDM group randomly, respectively. All processes involving animal treatments in this study were in accordance with the procedures of Ethical Committee for Animal Experimentation, Jinan University.

Immunofluorescent staining

Whole fetuses were photographed and then fixed in 4% paraformaldehyde. They were then dehydrated, embedded in paraffin wax and serially sectioned at 4 μm. Transverse sections of mouse fetal thoracic neural tubes were de-waxed in xylene, rehydrated and then heated in a microwave oven for antigen retrieval before exposure to the primary antibody, with citrate buffer (pH=6.0). Nonspecific immunoreactions were blocked using 5% inactivated goat serum in PBS for 60 min at room temperature. The sections were washed in PBS and incubated with Olig2, GFAP, NF-M, Tuj1, Ki67, Sox2, PCNA, CNTF, CT-1 and LIF overnight at 4°C. Following extensive washing, the sections were incubated in Alexa Fluor 555 anti-rabbit IgG or Alexa Fluor 488 anti-mouse IgG for 2 hours mostly at room temperature in a dark box. Eventually, the sections were counterstained with DAPI for 30 min at room temperature. The sections were photographed using fluorescent

microscope (Olympus BX53, Tokyo, Japan) that was linked to the cellSens Standard 1.9 software. A minimum of randomly 5 images from 3 samples were assayed per group. The percentage of positive cells from immunostaining assay was chosen and calculated automatically using Image Pro Plus 7.0 software. Tuj1, NF-M, GFAP, CNTF, LIF, CT-1 positive areas were quantified by measuring the areas of immunofluorescence signals with Image Pro Plus 7.0 software.

Western blot

Western blotting was performed in accordance with a standard procedure using a polyclonal antibody that specifically recognized NF-M, Tuj1, GFAP, p62 and CT-1. The collected developing mouse fetal neural tubes were frozen in liquid nitrogen and kept at -80°C. Protein from the mouse fetal neural tubes was isolated from tissue homogenates using a radio-immuno-precipitation assay (RIPA, Sigma, MO, USA) buffer supplemented with protease and phosphatase inhibitors. Protein concentrations were quantified with the BCA assay. The extracted protein was separated by 10% SDS-PAGE and transferred onto a polyvinylidene difluoride (PVDF) membrane (Millipore, MA, USA). The membrane was blocked with 5% non-fat milk and then incubated with NF-M, Tuj1, GFAP, CT-1, p62, β-actin and GAPDH in a TBST buffer at 4°C overnight. After incubation with the secondary antibody, either HRP goat anti-rabbit IgG or HRP goat anti-mouse IgG, the blots were developed with SuperSignalTM West Femto Chemiluminescent Substrate (ThermoFisher, Rockford, USA), Gel Doc™ XR+ System (Bio-Rad, CA, USA). Quantity One (Bio-Rad, CA, USA) software was used to capture the chemiluminescent signals and analyse the data.

RNA isolation and quantitative PCR

Total RNA was isolated from mouse fetuses using an E.Z.N.A.® Total RNA Kit (OMEGA, Georgia, USA) according to the manufacturer's instructions. First-strand cDNA synthesis and the SYBR® Green quantitative PCR (qPCR) assay were performed using the PrimeScript™ RT reagent Kit with gDNA Eraser (Takara, Shiga, Japan). The reverse transcription and amplification reactions were performed in C1000 Touch™ Thermal Cycler (Bio-Rad, USA). The cDNAs were amplified at 95 °C for 2 min for initial denaturation step and followed by 40 PCR cycles (95 °C for 15 seconds, 60°C for 30 seconds). The corresponding relative mRNA expression was normalized to GAPDH and was calculated using the 2−ΔΔCq method. The qPCR results were representative of three independent experiments. Primers for *GAPDH* are as follows: 5-TCAAATGGGCAGATGCAGGT-3 (forward); 5-AGCTGAGGGAGCTGAGATGA-3(reverse); Primers for *NF-M* are as follows: 5-AGCAGCTACCAGGACACCA-3 (forward); 5-AATCTGGTCTCTTCCCCCTCT-3 (reverse); Primers for *Tuj1* are as follows: 5-ACAATGAGGCCTCCTCTCAC-3 (forward); 5-TCCGTATAGTGCCCTTTGGC-3 (reverse); Primers for *Olig2* are as follows: 5-GAACCCCGAAAGGTGTGGAT-3 (forward); 5-TCAACCTTCCGAATGTGAATTAGA-3 (reverse); Primers for *GFAP* are as follows: 5-ACCTGCAGGAGTACCAGGAT-3 (forward); 5-CTTTTGCCCCCTCGGATCT-3 (reverse); Primers for *CNTF* are as follows: 5-GTAGGGTTGACCCACGTATGA-3 (forward); 5-AGGGTAAAGCACTAAGGTGGAAG-3 (reverse); Primers for *CT-1* are as follows: 5-CGGGTGAGTTGGGAGAAAGA-3 (forward); 5-GTCAGTCTGGTGGTCTTCCAT-3 (reverse);

Primers for *LIF* are as follows: 5-AGCTTGCAAACTCCGGCCA-3 (forward); 5-AAGGGCACAATCCCTGCATC-3 (reverse); Primers for *Sox2* are as follows: 5-TGGACTGCGAACTGGAGAAG-3 (forward); 5-AGTCGGCATCACGGTTTTTG-3 (reverse); Primers for *Nrf2* are as follows: 5-GAAAAGGAAAGAGCAAGAGCAACT-3 (forward); 5-TATCCAGGGCAAGCGACT-3 (reverse); Primers for *HO1* are as follows: 5-ATCCAACGACGTGGAGATCAG-3 (forward); 5-ATCTGCACCTTTCCTTTGCAG-3 (reverse); Primers for *SOD2* are as follows: 5-CTCCACAACATTTGAGGACGG-3 (forward); 5-CCCCTTGATGCTGGACTGTT-3 (reverse); Primers for *NQO1* are as follows: 5-GAGTCAGATTACAGACCCCAGG-3 (forward); 5-AATGGGCCCAGCTCGGAAG-3 (reverse); Primers for *p62* are as follows: 5-CAGATAGGCACGTGGGTGAC-3 (forward); 5-CCATGGTACGGCCAATGATG-3 (reverse).

Primary culture of neural stem cells and differentiated cells

The methods of neural stem cell isolation, incubation and neural differentiation were performed according to Sharon et al study [3]. In brief, the hippocampi were removed from the brain of postnatal day 1 mice and transferred to a 35-mm plate containing PBS with 2% d-glucose on ice. The hippocampi were resuspended in NSC medium and triturated with a fire-polished glass pipet (Brainbits, IL, USA). Subsequently, the supernatant containing single cells was pipetted off into a fresh tube, centrifuged, supernatant was removed and the cells were resuspended in neural stem cell (NSC) medium, cells were seeded at a density of 2 x 106 cells per 10 ml. The cells were cultured in a humidified incubator with 5% CO2 at 37°C in T-25 cm flask with NSC medium containing DMEM/F-12 (Gibco, China) supplemented with 2% B27 (Gibco, USA), 20 ng/ml of rmEGF (Gibco, CA, USA), 20 ng/ml of rmbFGF (Gibco, USA) and exposed to various concentrations of glucose (5.5 mmol/l, 25 mmol/l, 50 mM d-glucose, Sigma, MO, USA) with 5.5 mmol/l d-glucose acting as a control. After a 7-day incubation, the neurospheres were photographed using inverted microscope (Nikon Eclipse Ti-U, Tokyo, Japan) that was linked to the NIS Elements F3.2 software, then NSC medium was replaced by differentiation medium, which containing DMEM/F-12 (Gibco, China) supplemented with 1% fetal bovine serum (Gibco, Australia) and 2% B27 (Gibco, USA), to induce neural differentiation. After another 7-day incubation, the immunofluorescent staining was performed in the differentiated cells against Olig2, GFAP, NF-M, Nrf2, CNTF, and phospho-STAT3 (p-STAT3). CNTF (Gibco, PHC7015, USA) and ML385 (Sigma, SML1833, Singapore) were added to neural stem cell medium and differentiation medium at a final concentration of 20 ng/ml or 2.5 μg/ml, and ML385 was added to culture medium 72 hours before cells were harvested. The cells were photographed using confocal fluorescence microscopy (Olympus BX61, Tokyo, Japan) that was linked to the cellSens Dimension 1.16 software. A minimum of 5 images were assayed per treatment group.

Neurospheres were collected and fixed in 4% PF, followed by dehydrated, embedded in O.C.T (Sakura, USA) and serially sectioned at 15 μm. Then the immunofluorescent staining was performed in the sections against Nestin, Sox2 and Nrf2 respectively. The sections were photographed using confocal fluorescence microscopy (Olympus BX61, Tokyo, Japan) that was linked to the cellSens Dimension 1.16 software. A minimum of 5 images were assayed per

treatment group.

Flow cytometry assay

Intracellular ROS was determined using a non-fluorescent dye DCF-DA (2′,7′-dichlorodihydrofluorescein diacetate) (Sigma, USA), which is oxidized by ROS to the fluorescent dye DCF (2′,7′-dichlorofluorescin). The control and high glucose (25 mmol/l) treated neural stem cells were incubated in 10 μM DCF-DA for 20 min. Fluorescence was measured with a BD FACSAria (USA).

Transmission electron microscopy

The hippocampi of E15.5 fetal mice were fixed with 2.5% glutaraldehyde (G849973, Macklin) in 0.1 mol/l PBS for 2 hours, and then sent to the TEM Laboratory of Jinan University to detect mitochondria using transmission electron microscope (FEI TECNAI12, USA). The embedding, ultrathin sectioning and staining were performed by professional technicians.

Bioinformatics analysis

For the protein–protein interaction (PPI) network analysis, STRING (Search Tool for the Retrieval of Interacting Genes/Proteins, https://string-db.org) was used.

Data analysis

Statistical analysis was performed using SPSS 13.0 statistical package program. Constructions of statistical charts were performed using a Graphpad Prism 5 software package (Graphpad Software, CA, USA). Data were presented as means ± SD. All data were analyzed using ANOVA, LSD and SNK or *t* text, which was employed to establish whether there was any difference between the control and experimental data. $p<0.05$ was considered statistically significant.

Supplemental References

1. Kumar, S.D., S.T. Dheen, and S.S. Tay, *Maternal diabetes induces congenital heart defects in mice by altering the expression of genes involved in cardiovascular development.* Cardiovasc Diabetol, 2007. **6**: p. 34.
2. He, M.-Y., et al., *Nrf2 signalling and autophagy are involved in diabetes mellitus-induced defects in the development of mouse placenta.* Open biology, 2016. **6**(7): p. 160064.
3. Louis, S.A. and B.A. Reynolds, *Generation and differentiation of neurospheres from murine embryonic day 14 central nervous system tissue.* Methods Mol Biol, 2005. **290**: p. 265-80.